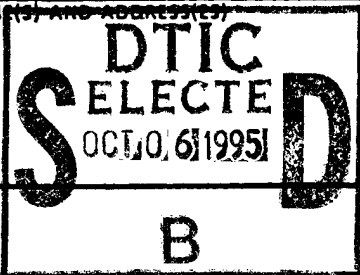


# REPORT DOCUMENTATION PAGE

Form Approved  
OMB No. 0704-0188

Public reporting burden for this collection of information is estimated to average 1 hour per response, including the time for reviewing instructions, searching existing data sources, gathering and maintaining the data needed, and completing and reviewing the collection of information. Send comments regarding this burden estimate or any other aspect of this collection of information, including suggestions for reducing this burden, to Washington Headquarters Services, Directorate for Information Operations and Reports, 1215 Jefferson Davis Highway, Suite 1204, Arlington, VA 22202-4302, and to the Office of Management and Budget, Paperwork Reduction Project (0704-0188), Washington, DC 20503.

1. AGENCY USE ONLY (Leave blank)		2. REPORT DATE Dec. 6, 1994		3. REPORT TYPE AND DATES COVERED Final, 11/15/89 - 9/30/94	
4. TITLE AND SUBTITLE (U) Shock Enhancement and Control of Hypersonic Combustion				5. FUNDING NUMBERS PE - 61103D PR - 3484 SA - AS G - AFOSR 90-0188	
6. AUTHOR(S)  Frank E. Marble and Edward E. Zukoski					
7. PERFORMING ORGANIZATION NAME(S) AND ADDRESS(ES)  California Institute of Technology Mail Code 205-45 Pasadena, CA 91125				8. PERFORMING ORGANIZATION REPORT NUMBER  AFOSR-TR-95  0601	
9. SPONSORING/MONITORING AGENCY NAME(S) AND ADDRESS(ES) AFOSR/NA 110 Duncan Avenue Suite B115 Bolling Air Force Base DC 20332-0001					
11. SUPPLEMENTARY NOTES					
12a. DISTRIBUTION/AVAILABILITY STATEMENT  Approved for public release; distribution is unlimited					
13. ABSTRACT (Maximum 200 words)  It is proposed to enhance the rate of mixing and combustion of hydrogen and air, and thereby reduce combustor length of scramjet combustors, through the introduction of streamwise vorticity generated by the interaction of a weak oblique shock wave with the density gradient between air and a cylindrical jet of hydrogen.  Because of the high Mach number flow in the combustor, the oblique shock traverses the jet at a very small angle and the principle of slender body theory allows one to replace the three-dimensional steady flow with a two-dimensional unsteady flow. As a consequence, two-dimensional time-dependent computational studies and an extensive experimental shock tube investigation were employed to assess mixing rates for the steady flow in the combustor. The results indicated that under realistic conditions, adequate mixing could be accomplished within one millisecond.  A "practical" injector, utilizing shock enhanced mixing, was designed for a combustor having a free stream Mach number of 6.0. A detailed aerodynamic and mixing investigation was carried out in the Mach 6 High Reynolds Number Tunnel at the NASA-Langley Research Center. The results confirmed both the details and the overall effectiveness of the shock enhanced mixing concept.					
14. SUBJECT TERMS  Supersonic Combustion, Vortex Combustion, Shear Layers, Vorticity Generation, Hypervelocity Mixing, Shock Enhanced Mixing				15. NUMBER OF PAGES 50 pp	
				16. PRICE CODE	
17. SECURITY CLASSIFICATION OF REPORT Unclassified	18. SECURITY CLASSIFICATION OF THIS PAGE Unclassified	19. SECURITY CLASSIFICATION OF ABSTRACT Unclassified	20. LIMITATION OF ABSTRACT UL		

NSN 7540-01-280-5500

Standard Form 298 (890104 Draft)  
Prescribed by ANSI Std. Z39-18

DTIC QUALITY INSPECTED 5

# 1. INTRODUCTION

The present report completes nearly eight years' work investigating the concept of shock enhancement of mixing and combustion rates specifically relating to gaseous hydrogen in air for supersonic conditions and the scramjet environment. I, along with others who may be a bit more objective than I, believe that the work was quite successful, a result which accrued from both the devoted efforts of the participating faculty and students at the California Institute of Technology and the enthusiastic support of Dr. Julian Tishkoff of the Air Force Office of Scientific Research.

Because of both its promising results and its timeliness, the program had a wider range of influence than many. It stimulated efforts to extend the concept of shock enhanced mixing at other research institutions and developed an interest within the NASP community that led to wind tunnel experiments that we carried out at the NASA-Langley Research Center. As a consequence I have felt it appropriate to review not only the work done directly under AFOSR sponsorship, but also to review briefly work directly spawned by that effort. Central among these were our own experiments at Langley, encouraged by Dr. Dennis Bushnell, on what we have called a "practical" injector.

A considerably shortened version of this work will appear as the Hottel Lecture of the 1994 International Combustion Symposium, Marble (1994).

Accession For		DATE
NTIS	GRA&I	<input checked="checked" type="checkbox"/>
DTIC	TAB	<input type="checkbox"/>
Unannounced		<input type="checkbox"/>
Justification		
By		
Distribution		
Availability Codes		
Dist	Avail and/or Special	

RESEARCH (AFSC)  
TIC  
has reviewed and is  
to IAW AFR 190-12

Approved for public release,  
distribution unlimited

## 2. ORIGINS OF THE SUPERSONIC COMBUSTION PROBLEM

Airbreathing propulsion at speeds exceeding 4 kilometers per second, that is Mach numbers of 12 or higher, encounters some novel and troublesome constraints on the combustion problem, e.g Ferri (1973), Kumar, Bushnell and Hussani (1989). To keep structural loads at acceptable levels, flight at such speeds is confined to high altitudes, 30 kilometers and higher, and in order to support reasonable combustion, the air pressure must be increased in the diffuser to about one atmosphere from its ambient value of  $1/100^{\text{th}}$  atmosphere. To be specific, travelling at Mach number 18 at 36 kilometers altitude requires decelerating the air to Mach number 6.0 to achieve a combustion pressure of one atmosphere, using a good diffuser and accounting for deviations from ideal gas. At the same time, the temperature of the air, initially at  $231^{\circ}\text{K}$ , has risen to  $1814^{\circ}\text{K}$ , a range where substantial structural cooling is necessary.

Now if  $h_o$  is the enthalpy of the air at flight altitude, the stagnation enthalpy as seen by the engine moving at a speed  $V_o$  is

$$H_o = h_o + \frac{1}{2} V_o^2 \quad 1.$$

a quantity which is conserved during the compression process. One of the features of high speed flow is that the kinetic energy, the second term of Eq. 1, is much larger than the thermodynamic enthalpy, in our case 50 times as large. Thus when the air speed is retarded to a value  $V$ , the enthalpy increases to a value  $h$  and, because the sum of these terms is conserved,

$$h - h_o = \frac{1}{2} (V_o^2 - V^2) \quad 2.$$

But because of the enormous difference in the magnitudes of the kinetic energy and the thermodynamic enthalpy, a very great increase in thermodynamic enthalpy results from a rather small fractional decrease in relative air velocity. For our example the nine-fold increase in air temperature involves a decrease in relative air velocity from the free-stream value of about 5586 m/sec only to 5094 m/sec entering the combustor.

At this velocity a combustion residence time of only one millisecond involves a flow length of five meters and a correspondingly large surface area to be cooled. Even a modest additional reduction in this velocity results in an increase in air pressure and temperature that seriously increases the surface cooling load. But the most compelling reason to avoid further velocity reduction is the increase in nozzle entrance temperature and the molar fraction of OH that accompanies this velocity reduction. The calculations shown in Table 1, made using a procedure and code developed by Serdengecti (1992), are very instructive in this regard.

Table 1. Combustor Conditions for Flight Mach Number 18  
Inlet Pressure One Atmosphere at Mach Numbers of 6.0 and 4.5

$M_4$	$z(\text{km})$	$V_4(\text{m/s})$	$T_4\text{K}$	$T_5\text{K}$	OH	$I_{sp}$
6.0	31.5	5185	1499	2612	0.011	1068
4.5	53.7	5224	2909	3014	0.039	658

The flight Mach number is 18 and the pressure in the combustion chamber is chosen to be one atmosphere. With a combustor Mach number of 6.0 and a combustor pressure of one atmosphere, the vehicle must fly at an altitude of 31.5 kilometers. Air enters the combustor with a velocity of 5185 m/sec and, for hydrogen fuel at a stoichiometry of 1.2, the products leave the combustor with a temperature of 2612 K. For chemical equilibrium at this temperature and pressure the mole fraction of OH at the combustor discharge is 0.011 and the resulting fuel specific impulse is 1068 seconds. It is this high specific impulse that establishes the value of the air breathing hypersonic engine.

If, however, we chose to drop the combustor inlet Mach number to 4.5, several significant changes take place. First, in order to keep the combustor pressure at one atmosphere, the flight altitude must be increased to nearly 53.7 kilometers and the ambient air temperature is increased from 231 K to 271 K. This Mach number reduction, in addition to increasing the ambient air temperature, leads to a much higher diffuser exit temperature and a 400 K increase in combustor discharge temperature over that for the Mach 6 combustor. As a consequence the mole fraction of OH in the combustion products increases dramatically to 0.039 and the fuel specific impulse drops to 658 seconds. This value is barely interesting and would not justify the attending complication of an air breathing engine.

In this regard it should be noted that the combustor inlet velocity is scarcely changed and remains at a value such that a combustor length of five meters provides a residence time of only a millisecond. This must be recognized as a serious constraint on the combustor because the gas temperatures we have found require intensive wall cooling which in turn mandates large heat capacity of the fuel. If the time required for fuel injection, mixing, and chemical reaction requires a long combustor, the cooling load exceeds the heat capacity available in the liquid hydrogen fuel used for the 1.2 times stoichiometric mixture. The additional hydrogen, regardless of how cleverly it is used, further reduces the fuel specific impulse and correspondingly compromises the the performance of the scramjet.

The foregoing factors thus set the injection, mixing and reaction constraints on the scramjet. Above all, the mixing must be very rapid; the injection must be accomplished with very low drag penalty, and the fuel must be distributed reasonably well over the burner cross section.

### 3. GENERATION OF STREAMWISE VORTICITY

The mixing of two parallel gas streams in a shear layer and the augmentation of this mixing rate by the introduction of streamwise vorticity are among the classical problems of fluid mechanics. Throughout the development of technical fluid mechanics a wide variety of devices, vortex generators, have been employed to create streamwise vorticity, usually to promote mixing within boundary layers to delay or avoid separation. When, however, such devices are placed further away from the wall in a very high velocity stream, their survival is jeopardized by very high heating rates even when they are cooled through their function as fuel injectors. Such devices may further introduce significant total pressure losses into the engine flow stream and deteriorate its performance, considerably so at combustor Mach numbers of 2.5 and above. In spite of these obstacles very effective combined fuel injectors and vortex generators which span the combustor stream have been developed and have proven very effective for combustors appropriate to flight Mach numbers as high as 10, Northam et al (1989).

The difficulties encountered in proceeding to higher speeds encourages the exploration of other techniques, preferably non-invasive techniques, to generate streamwise vorticity. The most familiar of the vorticity generating mechanisms involve either viscous torque which, is applied to a fluid element that undergoes a shearing motion, or the vortex sheet shed from a lifting surface along which the lift distribution is not uniform. The vortex generators mentioned earlier are of the latter type. In both of the above mechanisms of vorticity generation, solid surfaces within the fluid are required. The remaining mechanism for vorticity generation results from the interaction between variable pressure and variable density fields; the rate of vorticity generation is equal to

$$- \text{grad} \left( \frac{1}{\rho} \right) \times \text{grad} p \quad (3)$$

Because we are dealing with a flow field having adjacent streams of hydrogen and air, we may anticipate large values of  $\text{grad} \rho$  and hence the opportunity for strong vorticity generation. The mechanism through which this vorticity is created, Hendricks (1986), Marble and Hendricks (1986), Picone and Boris (1988), Picone et al (1983), will be of interest later and, because it is not obvious, it merits a brief discussion.

Figure 1, shows a rectangular fluid element, stratified in the direction indicated by  $\text{grad} \rho$  as well as by the hatching lines, so that the center of mass of the element lies above and to the right of the geometric center. The pressure gradient is shown in the horizontal direction, the pressure  $p$  acts on the left face, pressure  $p + \delta p$  acts on the right face where  $\delta p > 0$ . The resulting clockwise moment -or torque- about the center of mass is of magnitude proportional to

$$|\text{grad } \rho| |\text{grad } p| \sin \phi$$

(4)

where  $\phi$  is the angle between the two gradient vectors, and generates a distribution of negative vorticity within the element.

We propose to generate streamwise vorticity utilizing the density gradient at the interface between air and hydrogen fuel interacting with the pressure gradient created by an oblique shock wave. To fix our ideas consider the configuration shown in Fig. 2. Air flows supersonically over the combustor wall which, at one point, bends sharply into the flow through a small angle  $\delta$ , creating a weak oblique shock wave. Ahead of the shock wave a cylindrical stream of hydrogen flows parallel with the air stream and at the elliptical intersection with the shock turns slightly upward. It is at this intersection that the pressure and density gradients coexist and the progress of the two gradient vectors as the shock passes through the jet is shown in several cross sections, looking upstream into the flow. The density gradient lies in the plane and is radial to the slightly diffused air-hydrogen interface; the pressure gradient, normal to the shock wave front, lies slightly out of the plane. The vorticity generated at the intersection of these two regions is predominantly in the streamwise direction. The small azimuthal component of vorticity, lying on the surface of the hydrogen cylinder, will be neglected in our discussion because for air Mach numbers of interest the shock angle is very flat and this vorticity component correspondingly small.

As the shock intersection moves up through the jet, the magnitudes of the gradient vectors remain constant but the angle between them, equal to the angle of the radial line from the jet axis to the point of intersection, increases from  $\phi = 0$  as the shock enters the jet to  $\phi = \pi$  as it passes out at the top. The magnitude of the vorticity deposited at the intersection of the property gradients is proportional to the sine of this angle and its sense may be determined from Eq. 3. The resulting distribution of vorticity at the air-hydrogen interface is shown in a set of diagrams immediately below the sketch in Fig. 2. From this view clockwise vorticity is accumulated on the right half of the cross section and counter clockwise vorticity on the left half. The mixing enhancement contributed by the streamwise vorticity manifests itself as the induced distortion of the hydrogen jet. The progress of this distortion is sketched qualitatively in Fig. 3 as it proceeds from the distribution of vorticity, as it exists immediately after the shock has passed through the hydrogen jet, to the distortion induced by this vorticity a short time subsequent to shock passage. Because the vorticity distribution is antisymmetric about the vertical axis, the velocity field is antisymmetric also and the composition contours symmetric. The configuration is suggestive of a vortex pair and can be expected, in first approximation, to behave like one. Air is swept from below to the interior of the jet while the hydrogen in the upper portion of the field is stretched into a thin sheet joining the two vortices. Accompanying this is the large increase of interfacial area through which the diffusion requisite for molecular mixing takes place.

Several features of this configuration allow substantial analysis of the flow field details. First, for airflow at  $M = 6.0$  and conditions tabulated in section 2, it takes only about 50 microseconds for the shock to traverse a 5.0 cm diameter hydrogen jet. This is just 5% of the residence time of one millisecond in the combustion chamber. The displacements of the cylindrical geometry during this period are small so that we can assume an initial state to be the circular cylinder with the vorticity distribution calculated from the initial interaction and the shock itself out of the picture. Second, because the changes along the direction of flow involve little variation in streamwise velocity, plane sections normal to the stream remain approximately plane so that the distance and time can be interchanged. This transformation is quantitatively

$$t = \frac{x}{U} \quad (5)$$

where  $U$  is the uniform streamwise velocity. The transformation of certain steady three-dimensional flow fields into two-dimensional unsteady flows is known in this particular form as slender body theory, widely used in aerodynamic analysis, Sears (1954).

The transformation of this problem from a three-dimensional steady flow to a two-dimensional unsteady one allows:

- a) Two-dimensional Euler calculations of the progressive distortion of the shape and of the entire gas-dynamic field.
- b) Shock tube experiments of the distortion and mixing of cylindrical light gas masses subjected to weak shock waves.

Recognition of this possibility brings the problem within modest experimental and computational resources without requiring extensive and expensive facility investment. It was our good fortune that these virtues were also recognized by AFOSR and by Dr. Julian Tishkoff in particular to whom we are grateful for both enthusiasm and financial support.

## 4. SHOCK TUBE EXPERIMENTS

The bulk of the experimental investigation was performed in the Galcit 17-inch Shock Tube, Liepmann et al 1962. This same facility was utilized by Haas and Sturtevant 1987 in their study of shock interaction with gas inhomogeneities and our initial approach built upon their experience, Haas 1984. As our investigation developed, however, a quite different and novel approach was developed, Jacobs 1992, that will be described briefly.

The shock tube, 17 inches (43.18 cm) in diameter was fitted with a 60.69 cm long, 26.67 cm square test section with a transition from round shock tube to square test section accomplished using a 152.4 cm long "cookie cutter", Fig. 4. A pair of 15.24 cm diameter windows provided visual access to the test section; pressure taps fitted with piezoelectric pressure transducers provided timing signals needed to measure shock strength as well as to synchronize the experiments.

A large part of our experiments utilized planar laser-induced fluorescence (PLIF) in which helium is seeded with a small amount of biacetyl (Epstein 1977) and then made to fluoresce with a sheet of laser light. Thus, cross-sectional views of the three-dimensional density field are obtained. Biacetyl is a gaseous fluorescent dye with an absorption peak at 425 nm and a fluorescence peak at 460 nm. The fluorescence of biacetyl has been found to be fairly independent of temperature and insensitive to quenching (Epstein 1974), making the intensity of fluorescence linearly dependent upon the incident radiation and dye concentration. Thus the PLIF system could be used to measure species concentration.

A round laminar helium jet was introduced into the test section through a 0.794 cm diameter copper tube that entered through the sidewall of the test section and terminated in the central portion of the test section, allowing the jet to convect vertically upward, within the view of the lower window. A second piece of tubing, having a 1.9 cm opening, was situated directly above the jet to collect the light gas and ensure that excess helium did not accumulate in the test section. A portion of the helium was bubbled through liquid biacetyl, seeding the helium with nearly saturated vapor. A ratio of ten parts pure helium to one part biacetyl-laden helium was used in the experiments, which guaranteed that the addition of biacetyl to the helium stream would not increase the mixture density by more than 10%.

A Candella SLL-1050M flashlamp-pumped dye laser, filled with Exiton LD423 laser dye, provided 100 mJ pulses of 0.7  $\mu$ s duration at 430 nm. The resulting 18 mm beam was first passed through a 450 nm short-pass filter, then focused using a set of circular and cylindrical lenses to provide a sheet of laser light that bisected the biacetyl-seeded helium jet, illuminating a 1 mm thick cross section, Fig. 5. The resulting image was captured using a Xybion model ISG03 intensified CID camera, positioned to view upward through the lower test section window, and the output was sent to a Poynting Products PC-170 frame grabber. Because the flow behind the

shock wave translates the helium jet down the shock tube, the camera had to be positioned precisely at the location where the jet was expected to be when the laser was fired. The laser and the data acquisition systems were triggered using pressure signals produced by the incident shock, fed to two Stanford Research DG535 digital delay generators which produced signals necessary for coordination of the laser firing, frame grabber triggering and camera gating.

Figure 6 shows the PLIF images of the distorted helium cylinder, initially of 0.66 cm diameter, resulting from interaction with a weak shock of Mach number 1.093. This corresponds essentially to a Mach wave in a combustor having a throughflow Mach number of 6.0. The false coloring, as indicated in the color bar, extends from white, representing the lowest fluorescent intensity, to yellow, representing the highest. Because the optical system could produce only a single image each firing of the shock tube, the images are from separate shots, fitted together in a time sequence.

The images 6b and 6c, 0.128 ms and 0.273 ms respectively after the encounter, exhibit the character inferred by our earlier sketches of the phenomenon. The vorticity deposited at the boundary rolls up into a distinct vortex pair, the individual lobes moving apart extending the fine "umbilical cord" that joins them. From the viewpoint of mixing, the extension of the interfacial area and the thinning of the interfacial zone due to straining are the crucial items.

Beginning with the fourth frame, 6d, a further development becomes evident. A second lobe develops, further extending the interfacial area. This second lobe appears to mix much more rapidly than the original vortices, essentially disappearing by the frame 6g 0.773 ms after the encounter. In Fig. 6h, after 0.973 ms, the secondary lobes and the umbilical cord are thoroughly mixed but a remnant of the original vortex persists. The fact that the time of the final frame is very close to the residence time we had set for the combustion chamber should not be taken seriously because this time scales with the physical properties of the gases and particularly with the shock strength and the sonic velocity.

It is instructive to examine the mixing process as indicated by the PLIF images and to segregate, roughly, the mixing rates in each of the lobes; this is shown in Fig. 7. This simple dimensional plot indicates that when the two lobes are first discernible, the primary lobe contains about 60 % of the helium, the secondary lobe containing the remainder. After about one millisecond the secondary lobe is completely mixed and the primary lobe is about 40 % mixed. Although we may conjecture about the reasons for the contrasting behavior of the two lobes, the PLIF images alone cannot resolve the issue. This must rely upon computations that will be discussed subsequently.

One concern about the experiments employing laser induced fluorescence with the biacetyl dye has to do with the differences in diffusion rates of the relatively heavy biacetyl molecule compared with that of helium. As a consequence, the dynamics of the distortion and mixing are well represented but the diffusion component may be underestimated. Because it is the diffusion component that provides molecular mixing required for chemical reaction, it is important to discern significant effects that may not be accurately reproduced in Jacobs' results.

As a consequence a very similar program utilizing Rayleigh scattering was undertaken, the results of which appear in Budzinski et al (1992) and in Budzinski (1992). The Rayleigh scattering technique differentiates between air and helium through the very much larger scattering cross section of oxygen and nitrogen compared with that of helium. As a result the molar concentration of the species themselves may be followed without relying upon a foreign tracer molecule.

Budzinski's experiments using Rayleigh scattering were performed with the same shock tube and essentially the same instrumentation used by Jacobs (1992). The significant differences were that the laser beam was tuned to a wave length of 480 nm and a Star I cooled CDC camera was employed having an array of 576 by 384 square pixels, each 20 microns on a side. A set of these results at a shock Mach number of 1.066 is shown in Fig. 8. Although detailed comparison with the earlier PLIF measurements, Fig. 6, is not straightforward because of differences in initial jet radius and shock Mach number, some features are clear. First, the general course of the distortion and rolling up process recorded by Jacobs is well confirmed. Second, the true extent of the diffusion zones is much greater than suggested by the PLIF images. This feature was to be expected and, indeed, was the motivation for repeating the experiment utilizing Rayleigh scattering. The contrast is clear from the Rayleigh image of the initial jet, Fig. 8a, where the significant helium gradients within the jet were not apparent in the PLIF images. The extent of the diffusive mixing as the distortion proceeds is indicated in Fig. 9 where the distribution of helium mole fraction is plotted for two cuts through the vortex and tail regions of the image shown in Fig. 8d. Even in this rather early time in the mixing process, it is clear that the helium mole fraction has been reduced to 0.5 or less in all except the core of the original vortex and the innermost portion of the tail. This result supplies a quantitatively more accurate account of the extent of molecular mixing than we were able to deduce from the PLIF measurements. Again, the difference in mixing of the tail and the main vortex core as the process proceeds, is evident as initially shown by Jacobs experiments.

## 5. COMPUTATIONAL INVESTIGATION

An extensive computational program was undertaken in parallel with experiments just described. The aim was both to provide a guide to the experimental effort and to calculate additional flow quantities, such as pressure and vorticity, which could only be qualitatively inferred from the experiments. The progress was enhanced considerably when we were able to obtain from Eric Baum of TRW a code which he had modified from one that originated at the Naval Research Laboratory and had been used earlier to examine the early experiments of Haas (1984).

The code employed the Flux Corrected Transport algorithm developed by Boris et al 1973, 1975, which overcomes the tendency to develop oscillations in the presence of strong gradients by employing a diffusive differencing scheme. This, however, has a smearing effect in the vicinity of these large gradients, a problem which is solved by employing a second "antidiffusion" stage. In this way shock structures and contact surfaces between fluids of different density remain highly resolved and oscillations are not encountered. As modified by Baum, the code employs alternate direction splitting. For each time step all terms in the differential equations involving x-direction derivatives are integrated first along rows of constant y, followed by an integration of y-derivatives along columns of constant x. The problem at each time step therefore involves the solution of a succession of ordinary differential equations, leading to a significant simplification in programming.

In keeping with our invocation of slender body theory, we replace the three-dimensional steady problem with a two-dimensional unsteady problem. Further, the computations employed an inviscid, non-diffusive formulation and consequently any diffusive component to the results is purely numerical. Although the use of an Euler code in this investigation suppresses some features of the real process, it does calculate, and indeed emphasizes, certain structural features of the flow which are key to a deeper understanding of the experiments. These calculations, carried out by G.J. Hendricks during the spring of 1987, have been previously published only in part, Marble, Hendricks & Zukoski 1987a, 1987b, but were an essential part in understanding the mixing phenomenon in question. This type of calculation was repeated subsequently, with somewhat greater accuracy, by Yang et al (1993, 1994), Yang & Kubota (1994).

Figure 10 shows a sequence of composition (density) distributions from Hendricks' numerical calculations of a Mach 1.22 shock passing over an initially circular cylinder of helium in air. Because of its symmetry with respect to the horizontal center line, only the upper half of the vortex pair is shown. The times have been selected to show the formation of the two lobes and their further development. To put these calculations in correspondence with the PLIF images in Fig. 6, the calculation for 1.09 ms, Fig. 10c, corresponds approximately to Fig. 6d. One sees evidence of the tendency to form two lobes beginning in Fig. 10b and quite developed in 10c. Figures 10d through 10f illustrate the formation and stretching of the rearward lobe but,

because of the absence of diffusive mixing, this lobe does not disappear as in the PLIF images, but retains its strongly distorted boundary.

The mechanism of the process is greatly clarified by examination of the pressure and vorticity diagrams corresponding to the composition plots of Fig. 10. Figures 11, 12, 13 present vorticity and pressure diagrams corresponding to the composition diagrams of Fig. 10b, 10c, and 10e respectively. Quite early in the development, Fig. 11 shows the vorticity to be moving to the forward position of the structure and the closed contours of the pressure distribution suggest a well formed vortex. The forward movement of the highly vortical portion of the structure is thus associated with the motion of the corresponding vortex pair. The composition distribution of Fig. 12 shows the distinct separation of the two lobes and the corresponding vorticity distribution exhibits the continued differentiation between the vorticity density on the two lobes. The pressure distribution emphasizes the vortex structure of the forward lobe which continues to pull away from its trailing counterpart. The final set of diagrams, Fig. 13, shows the weak trailing "wake" which in physical reality would be experiencing the diffusive mixing shown in the PLIF images. The vorticity is now well formed into a relatively stable circular vortex structure. The pressure distribution shows this even more convincingly; the field of the forward portion is very much that of a classical vortex pair while the rear lobe has effectively vanished dynamically.

And now the reason for the longevity of the forward lobe is clear; it had formed a very stable stratified vortex and will maintain itself over a long period, mixing and dissipating very slowly. From a mixing point of view it is interesting to speculate on the merit of another disturbance to alter the flow before the vortex has stabilized.

Because different experiments and their various technological applications differ in gas properties, gas states as well as in shock strength and the diameter of the gas cylinder with which the shock interacts, one needs a rational means to compare the behavior of these situations. Because the detailed distortion of the gas cylinder is essentially inviscid and non diffusive, we may formulate the scaling principle neglecting these processes. Referring to Fig. 14, consider the cylinder of diameter  $D$  consisting of gas with properties  $a_2$ ,  $\gamma_2$  and gas external to the cylinder with properties  $a_1$ ,  $\gamma_1$ . A weak shock approaching from the left at Mach number  $M_s$  carries a pressure difference

$$\frac{\delta p}{\gamma_1 p_0} = \frac{2}{\gamma_1 + 1} (M_s^2 - 1) \quad 6.$$

and, from acoustic theory,  $\delta p / \gamma_1 p_0 = u_1 / a_1$ , where  $u_1$  is the gas velocity following the shock. After the shock meets the cylinder, the signal moves along the diameter a distance  $a_2 t$  and generates a horizontal velocity  $u_2$  in the region traversed. At the same time the incident shock is reflected a distance  $a_1 t$  back upstream and, because the gas medium is continuous at the interface, the gas velocity in this segment is  $u_2$  also. Away from the cylinder the shock generates a velocity  $u_1$  in the initially stationary gas and after the time  $t$  has penetrated a distance  $a_1 t$  downstream of the point of shock impingement on the cylinder.

The circulation  $\Gamma$  about the cylinder is easily calculated using the contour shown and is

$$\Gamma = u_2(a_2 t + a_1 t) - u_1(2a_1 t) \quad 7.$$

From one-dimensional acoustic theory we know that the gas velocity after the reflection may be expressed

$$\frac{u_2}{a_2} = \left( \frac{2}{\frac{\gamma_2}{\gamma_1} + \frac{a_2}{a_1}} \right) \frac{u_1}{a_1} \quad 8.$$

and the circulation, from Eq. 7, is

$$\Gamma = 2 a_1 u_1 t \left[ \frac{\left( \frac{a_2}{a_1} \right)^2 - \frac{\gamma_2}{\gamma_1}}{\frac{a_2}{a_1} + \frac{\gamma_2}{\gamma_1}} \right] \quad 9.$$

Finally, inserting the value of  $u_1$  from the pressure relation above and recalling that the acoustic velocity is  $a = \sqrt{\frac{\gamma p}{\rho}}$  where  $p$  is essentially uniform for this calculation, Eq. 9 becomes

$$\Gamma = 4a_1 D \left( \frac{a_2 t}{D} \right) \frac{M_s^2 - 1}{\gamma_1 + 1} \left( \frac{1 - \frac{\rho_2}{\rho_1}}{1 + \sqrt{\frac{\gamma_2 \rho_2}{\gamma_1 \rho_1}}} \right) \quad 10.$$

a result obtained by Hendricks in late 1986 when the computations described previously were done. At the time  $D/a_2$  the acoustic wave has penetrated to the downstream limit of the light gas and the circulation has reached  $\Gamma_*$ , very nearly its final value

$$\Gamma_* = 4a_1 D \frac{M_s^2 - 1}{\gamma_1 + 1} \left( \frac{1 - \frac{\rho_2}{\rho_1}}{1 + \sqrt{\frac{\gamma_2 \rho_2}{\gamma_1 \rho_1}}} \right) \quad 11.$$

Note that the circulation grows linearly in time

$$\Gamma = \Gamma_* \left( \frac{a_2 t}{D} \right) \quad 12.$$

until  $a_2 t = D$ . The comparison of these analytical results with the circulation growth evaluated from the calculations described previously, shown in Fig. 15, confirms their reasonable accuracy and establishes confidence in Eq. 10 through Eq. 12 as valid scaling laws.

The final circulation given by Eq. 11 may be used to determine a time scale for the kinematic distortion and roll-up of the vortex pair created by the interaction. The velocities induced by one vortex in its neighborhood are of the order  $\Gamma_*/D$  and hence the time  $t_*$  required to move the gas a distance comparable with the cylinder dimensions is then  $t_* = D^2/\Gamma_*$ . Using the circulation, Eq. 11, we may write explicitly

$$\frac{a_1 t_*}{D} = \frac{\gamma_1 + 1}{4} \frac{1}{M_s^2 - 1} \left( \frac{1 + \sqrt{\frac{\gamma_2 \rho_2}{\gamma_1 \rho_1}}}{1 - \frac{\rho_2}{\rho_1}} \right) \quad 13.$$

Both experimental and computational results have, to this point, involved fields without combustion. The effects of combustion may be classified in two categories: First, the alteration of gas properties, and second, alterations to the gasdynamic flow field associated with the change in gas density resulting from changes of molar composition and temperature. Numerical calculations for reacting flow fields have frequently been troubled by oscillations due to "stiffness" associated with the differential equations containing the chemical reaction terms. Recently several methods have been advanced to avoid this difficulty, one of which, the ENO (Essentially Non-Oscillatory) scheme, Harten et al (1986), Shu & Osher (1989), has been applied to study the combustion of hydrogen in air for the dynamic process we have been discussing.

For this computation the cylinder of hydrogen was situated in air at one atmosphere and at the same initial temperature; the kinematic conditions similar to both calculations and experiments that have been described. For hydrogen chemistry eight chemical species were followed ( $H_2$ ,  $H$ ,  $O_2$ ,  $O$ ,  $H_2O$ ,  $OH$ ,  $HO_2$ , and  $H_2O_2$ ) using the set of 37 reactions described by Maas & Warnatz (1988). The details of the formulation, including the determination of local transport properties, are described by Ton (1993) and by Ton et al (1994).

Figure 16 shows the rather striking dispersion of the density distribution by the reaction. Here the "source effect" of the heat release, described in a rudimentary way by Karagozian & Marble (1986) is clearly visible. In addition, those features observed in diagrams for non-reacting mixing, due only to variation in composition, are obscured here by those density variations controlled by temperature. For example, the separation into two lobes, so evident in the non-reacting development (cf Fig. 16b vs Fig. 16B) is largely obscured by the hot products outside the structure but may be discerned by the darkest contours within the diagram.

A second important point concerns the effect of initial mixture temperature upon the ignition and the ensuing combustion processes. A rather convincing comparison appears in Fig. 17 for the ignition and progress of early combustion at the initial temperatures of  $1000^\circ K$  and  $1500^\circ K$ . If we again trace the separation into two lobes for the three images at each temperature, very significant differences are evident. It is quite probable that higher

temperatures, particularly in the outer portions of the later images for the 1500° K initial temperature, are counteracting the stable stratification due to composition that was observed in the non-reacting computations and experiments. Indeed, if this observation is valid, the contribution of combustion may go a long way toward reducing the mixing and combustion times for the forward moving vortex pair.

Finally, from the viewpoint of combustor performance, the production and consumption rates of certain species are of interest. Figure 18 shows the time history for several species, for each of the initial temperatures, their masses integrated over the computational domain. The consumption of hydrogen shows clearly the ignition delay occurring at the lower initial temperature, the subsequent rapid reaction and consumption of hydrogen at a rate no longer sensitive to initial temperature. The ignition delay might be expected simply on the basis of temperature but it seems likely that a more complex process is involved. The very rapid reaction subsequent to the time delay suggests that a considerable amount of surface extension has taken place during the time and that reaction has been suppressed by the high straining rates involved in extending the hydrogen-air interface. Recent analytical studies of the effect of strain rate on ignition support this interpretation and the straining rates in the experiments and computations described are well in the range to play a role in the observed phenomenon. However, the present computations are sufficient only to support the possibility but not to provide conclusive demonstration.

## 6. TOWARD A PRACTICAL INJECTOR

At this stage of the investigation it appeared that the principle of shock enhanced mixing through generation of streamwise vorticity had been well demonstrated but its application in the harsh environment of a scramjet engine was yet another matter. It was evident that some innovation was required and a rudimentary sketch of our concept is shown in Fig. 19. The problem is to bring the hydrogen into the combustor with a low-drag configuration and then to impact it with a weak shock that imparts streamwise vorticity of the appropriate sense and lifts the jet away from the wall. Let us first examine the proposed configuration of the injector and then explore the gasdynamic issues computationally.

Air moves parallel to the combustor wall at a Mach number of 6.0. At one position the wall divides into alternating ramps and troughs; the air expands to a higher velocity within the troughs but generates weak compression waves above the ramps. The ramps are, in reality, channels guiding the hydrogen streams into the chamber, as shown in section B-B. Then the hydrogen jets discharge at section A-A where we see the open hydrogen passages and the hatched troughs carrying the high velocity air stream. Note that at this point there is a shearing motion between the downward-moving air and the upward-moving hydrogen, creating a vertical shear layer at the interface where the hydrogen and the air merge. This motion corresponds to a significant amount of streamwise vorticity at the hydrogen-air interface and care must be taken to insure that the shock enhancement augments rather than cancels this vorticity.

At the point of hydrogen discharge the combustor wall returns to its original direction, creating a weak oblique shock in the air leaving each trough. These shocks, in turn, establish locally high pressures that propagate into and upward through the hydrogen, driving it upward to create a recognizable analog of the shock-cylinder interaction studied in the shock tube.

Because the trough and ramp angles are very small, as dictated by the high Mach number flow, we may again analyze this three-dimensional steady flow field section by section as a two dimensional non-steady one. Computations were again performed by G.J.Hendricks utilizing essentially the same Euler code as used for the shock tube calculations, but with the obvious introduction of moving boundaries. The computational domain consisted of one complete geometric cycle in section A-A, Fig. 19. To model the streamwise motion over the ramps and channels, the height of the ramp stepped up while the trough stepped down. These movements generated the gas motion in the cross plane while still within the injector. Figure 20 shows the density contours for distances of 4.0 and 12.0 ramp widths from the location where the ramps and troughs began. Figure 20 shows, at 4.0 ramp widths, the Mach fan expansion in the top middle of the trough and the movement of the shock upward away from the ramp and into the free stream. Because of the pressure difference caused by the compression shock and the expansion wave, air flows from the top of the ramp, around the sharp corner and into the trough. The two corner flows meet at the center of the trough where they are forced to move parallel to the channel walls and compensate for the overexpansion about the corners. The shocks

propagating above the tops of the ramps begin to merge and form a wrinkled shock above the injector. At the end of the injector body, 12 ramp widths, Figure 20 shows the formation of the shock reflection mentioned above with the continued downward motion of the air into the trough. As we follow the gas plane along the flow path, the downward velocity of the air in that plane corresponds to a Mach number of about 0.6.

Passing beyond the plane at which the injector ends, two events change the nature of the flow. First, the restraints of the walls are removed and therefore the air and hydrogen are set in motion relieving the pressure difference previously existing across the injector walls. Second the oblique shock shown in section C-C of Fig. 19 is formed, causing an abrupt pressure increase below it. The resulting gas motion and composition patterns are shown in Fig. 21 where it must be noted that the domain shown has been shifted so that the emerging hydrogen jet occupies the center of the diagram.

At 14 ramp widths, 2.0 ramp widths downstream of the injector, Fig. 21 shows the shock wave generated in the air at the lower part of the trough propagating upward. At the same time, the higher pressure created under this shock is moving air under the hydrogen and displacing it upward. At a station of 20.0 ramp widths, 6.0 ramp widths downstream of the injector, Fig. 21, the symmetric shock waves under the hydrogen have reflected at the center point further increasing the pressure under the hydrogen and, most important, have created a vertical jet penetrating into the hydrogen flow, dividing it into two halves and generating the vortex pair corresponding to those observed in the shock tube studies. The concept of creating a vortex pair in the hydrogen flow and generating streamwise vorticity is now clear. By configuring the injector to build a shock that penetrates under the hydrogen jet, the shock then moves up through the hydrogen producing an almost identical phenomenon to that generated in the shock tube.

On the basis of numerical studies, examples of which we have seen, the injector shown in Fig. 21 was designed, closely resembling the original concept, Fig. 19. Caltech was allowed generous running time in the One Foot, Mach 6 High Reynolds Number tunnel at Langley Memorial Aeronautical Laboratory, giving us a rare opportunity to measure the workings of the injector in a physical situation that duplicated the actual event in all ways except for combustion. The success of this effort was assured by the good offices of Dr. Dennis Bushnell who enthusiastically supported the effort and more than once extracted us from bureaucratic tar pits, and by Ian Waitz, a graduate student at Caltech, who already had two years of valuable experience working at Langley.

The wind tunnel model, Fig. 22 and Fig. 23, although identical in concept to the original design for which the calculations have been discussed, had a spacing between injector ramps of three injector widths rather than a single injector width. This change was made for two reasons. First, the mass flow of hydrogen would have been too great for the closely spaced injector in a combustor of appropriate cross section. The second reason, equally compelling, was that both initial experiments and some of the Navier Stokes computations to be described presently, suggested that the flow of boundary layer air from the compression ramps into the troughs was sufficient to "soften" the compression shock at the injector outlet. Because this would compromise their performance, the spacing between injector lobes was increased by a factor of three, greatly reducing the possibility of boundary layer contamination.

The model injectors were installed as inserts on the flat plate rig, Fig. 23, the helium flowing into the individual injectors from a plenum supplied through the mounting strut supporting the plate. The strut also housed an air supply to a series of holes near the leading edge of the plate which could be activated, optionally, for controlling the boundary layer thickness or fixing boundary layer transition. Two geometrically similar injector inserts were used in the experiments, one having an injector height of 1.0 inch at the discharge plane, the other having an injector height of 0.5 inch. The requirement for the two models resulted from the maximum allowable length of the model in the tunnel. Since the non-dimensional distance downstream from the injector was measured in terms of the injector height, the smaller model gave the opportunity to extend the effective length of the mixing region that could be studied while the larger model provided greater resolution for measurements in the near field.

During the period of model manufacture, model installation and the model and instrumentation shakedown tests in the tunnel, a detailed computational investigation of the injector was undertaken. The main motivation for this effort was to obtain a good estimate of the mixing performance we should expect, to determine bounds on the range of densities and pressures to be expected, and to secure this information at a time when modifications of the instrumentation and the detailed test program could be made. These computations were done using the SPARK3D code, Ecklund et al (1990), provided by the Computational Methods Branch of NASA Langley Research Center. This code allowed solution for three-dimensional multi-species flows using Navier Stokes, energy and species conservation equations. The chemical reaction capability of the code was not used. The Mach numbers of the main stream and the helium jets were matched with those of the experiments. The similarity with the temporal development observed in the shock tube, including formation of the vortex pair, the development of the trailing lobes, and the motion of the strong vortex pair away from the wall and the trailing lobes, was striking. In spite of the fact that the shock incident on the helium jet is generated in a quite different manner than in the shock tube, the physical process develops as predicted.

Data acquired during the wind tunnel experiments consisted of three-dimensional surveys by four rake-mounted probes. These were: a composition probe, a cone static probe, a pitot probe, and a total temperature probe. Static pressure taps were located at a number of points in the flat plate following the injector discharge. The positioning of the probe rake, the pressure and temperature data, and the helium sampling, were automated. Helium concentration measurements were made with a composition probe, see Waitz (1991), Waitz et al (1993), based upon the response of a hot film anemometer sensor in a binary gas mixture. Care was taken by means of schlieren observation to assure that the sampling probe had swallowed the shock and thus to avoid preferential ingestion of the heavier molecular species. The resulting error of helium concentration measurements was less than  $\pm 3\%$  over the range of application. The response time was of the order of 1.5 seconds so that a complete concentration map at one streamwise position could be obtained in less than 5 minutes. The survey over ten cross sections required less than one hour, well within the blowdown time of the tunnel.

Figure 24 shows experimental contours of helium concentration at three locations downstream of the larger, or full scale, injector, Waitz et al (1992a, 1993). The experimental sampling grid is shown superposed on the contour plot for  $x = 8$ . This experimental

confirmation of the formation and development of the vortex pairs is again quite remarkable. For rough comparison with the sequence of density images, Fig. 6, obtained in the shock tube, the density distribution at  $x = 13$  occurs at a time of approximately 0.36 ms after leaving the injection plane at which time the maximum concentration was found to be 0.27, about a quarter of the original.

The corresponding computational helium concentration contours, Fig. 24, Waitz et al (1992b), compare very favorably with the measurements. The computational grid for the cross section is shown superimposed on the contour plot for  $x = 8$ . Some differences may be noted at  $x = 1$  where the experiments show the jet to be lifted and with somewhat more lateral spread, and as the vortex pair develops, the computed spread is somewhat less. The far field lifting of the vortex pair appears to be computed with reasonable accuracy. Finally, utilizing data from both the full size and half size models it is possible to trace the decay of maximum helium concentration along the flow path from the injector discharge to a point 26 injector heights downstream. This is shown in Fig. 25, the different symbols identify from which injector the data came. The agreement of the two data sets is very good in the range  $8 \leq x \leq 16$  but the agreement at  $x = 4$  is less satisfactory. It is difficult to sort this out conclusively, but the fact that the boundary layer thickness is numerically the same in both experiments may be a factor. Specifically, the ratio of the boundary layer thickness upstream of the injector to the ejector discharge height is 0.2 for the full size injector and 0.4 for the half size. The tendency for the helium concentration to maintain its initial value for the full size injector at  $x = 4$  is plausible from the concentration contours of Fig. 24, where we see that  $x = 4$  is the last point where the effect of the vortex pair is not in evidence.

If we interpret the results of Fig. 25 in terms of the full size injector, this final point at which 10% of the original helium concentration has been reached, the elapsed time at wind tunnel conditions, would be about 0.6 ms after a run of 26 inches. At the flight condition proposed in Section 2, this translates to a distance about four times this amount which is under three meters. This distance is well within the range of our initial goal for shock enhanced mixing.

## 7. NOTATION

$a$	Velocity of sound
$a_1$	Velocity of sound, air
$a_2$	Velocity of sound, light gas
$D$	Diameter of light gas jet
$h$	Enthalpy of air
$h_o$	Enthalpy of ambient air
$H_o$	Stagnation enthalpy of ambient air
$I_{sp}$	Specific impulse of scramjet
$M$	Mach number
$M_o$	Free stream Mach number
$M_4$	Mach number at combustor entrance
$M_s$	Mach number of flow normal to weak oblique shock
$p$	Pressure
$p_o$	Undisturbed ambient air pressure
$t$	Time
$t_*$	Time to develop full circulation of vortex pair
$T_4$	Temperature of air entering combustion chamber
$T_5$	Temperature of products leaving combustion chamber
$u_1$	Gas velocity in air following acoustic wave
$u_2$	Gas velocity in light gas following acoustic wave
$U$	Air velocity following shock in shock tube
$V$	Air velocity relative to scramjet
$V_o$	Undisturbed air velocity relative to scramjet
$V_4$	Relative velocity of air entering combustion chamber
$x$	Distance in direction of undisturbed flow
$z$	Altitude
$\gamma_1$	Specific heat ratio of air
$\gamma_2$	Specific heat ratio of light gas
$\Gamma$	Circulation of vortex pair generated by weak shock
$\Gamma_*$	Final circulation of vortex pair generated by weak shock
$\phi$	Angle about circular cylinder of light gas
$\rho$	Gas density
$\rho_1$	Density of heavy gas
$\rho_2$	Density of light gas

## 8. REFERENCES

Boris, J. P. and Book, D. L. (1973). Flux Corrected Transport. I. SHASTA, a Fluid Transport Algorithm that Works. *J. Comput Phys.*, 11, 38-69.

Boris, J. P., Book, D. L., and Hain, K. (1975). Generalization of the Flux-Corrected Transport Technique. *J. Comput. Phys.*, 18, 284.

Budzinski, J. M. (1992). Planar Rayleigh Scattering Measurements of Shock Enhanced Mixing. Ph.D. Thesis, California Institute of Technology, Pasadena, California.

Budzinski, J. M. , Zukoski, E. E., and Marble, F. E. (1992). Rayleigh Scattering Measurements of Shock Enhanced Mixing. AIAA Paper No. 92-3546.

Eklund, D. R., Northam, G. B., and Fletcher, D. G. (1990). A Validation Study of the Spark Navier Stokes Code for Nonreacting Scramjet Flowfields. AIAA Paper No. 90-2360.

Epstein, A. H. (1974). Fluorescent Gaseous Tracers for Three Dimensional Flow Visualization. MIT Gas Turbine Laboratory Report No. 117.

Epstein, A. H. (1977). Quantitative Density Visualization on a Transonic Compressor Rotor. *Trans. ASME, Vol. 99, Ser. A, No. 3. Jour. Engineering for Power*, pp 460-475.

Ferri, A. (1973). Mixing-Controlled Combustion. *Ann. Rev. Fluid. Mech.* 5, 301-338.

Haas, J-F. L. (1983). Interaction of Weak Shock Waves with Discrete Gas Inhomogeneities. Ph.D. Thesis. California Institute of Technology. Pasadena, California.

Haas, J-F. L., and Sturtevant, B. (1987). Interaction of Weak Shock Waves with Cylindrical and Spherical Gas Inhomogeneities. *J. Fluid Mech.*, 181, 41-76.

Harten, A., Osher, S. J., Engquist, B. E., and Chakravarthy, S. R. (1986). Some Results on Uniformly High-Order Accurate Essentially Non-Oscillatory Schemes. *J. Appl. Numer. Math.*, 2, 347-377.

Hendricks, G. J. (1986). Two Mechanisms of Vorticity Generation in Combusting Flow Fields. Ph. D. Thesis, California Institute of Technology. Pasadena, California.

Jacobs, J. W. (1992). Shock Induced Mixing of a Light Gas Cylinder *J. Fluid Mech.*, 234, 629-649.

- Karagozian, A. R. and Marble, F. E. (1986). Study of a Diffusion Flame in a Stretched Vortex. *Comb. Sci. and Tech.* 45, 65-84.
- Kumar, A., Bushnell, D. M., and Hussaini, M. Y. (1989). Mixing Augmentation Technique for Hypervelocity Scramjets. *AIAA J. Propulsion*, Vol. 5, No. 5, pp 514-522.
- Liepmann, H. W., Roshko, A., Coles, D., and Sturtevant, B. (1962). A 17-inch Diameter Shock Tube for Studies in Rarified Gas Dynamics. *Rev. Sci. Inst.*, 33, 625-631.
- Maas, U. and Warnatz, J. (1988). Ignition Processes in Hydrogen-Oxygen Mixtures. *Comb. and Flame*, 74, 53-69.
- Marble, F. E., and Hendricks, G. J. (1986). Behavior of a Diffusion Flame in a Flow Inducing a Pressure Gradient along its Length. *Proceedings, 21st International Combustion Symposium*.
- Marble, F. E., Hendricks, G. J., and Zukoski, E. E. (1987). Progress toward Shock Enhancement of Supersonic Combustion Processes. *AIAA Paper No. 87-1880*.
- Marble, F. E., Hendricks, G. J., and Zukoski, E. E. (1987). Progress toward Shock Enhancement of Supersonic Combustion Processes. *Turbulent Reactive Flows*, Rouen, R. Borghi & S.N.B. Murthy (Eds) pp 932-950.
- Marble, F. E. (1994). Gasdynamic Enhancement of Non-Premixed Combustion. *Proceedings, 25th Symposium, International Combustion Institute*, In publication.
- Marble, F. E., Zukoski, E. E., Jacobs, J. W., Hendricks, G. J., and Waitz, I. A. (1990). Shock Enhancement and Control of Hypersonic Mixing and Combustion. *AIAA Paper No. 90-1981*.
- Northam, G. B., Greenberg, I., and Byington, C. S. (1989). Evaluation of Parallel Injector Configurations for Supersonic Combustion. *AIAA Paper No. 89-2525*.
- Picone, J. M., Oran, E. S., Boris, J. P., and Young, T. R., Jr. (1983). Theory of Vorticity Generation by Shock Wave and Flame Interaction. *Prog. in Aero. and Astro.*, 94, 429-488.
- Picone, J. M. and Boris, J. P. (1988). Vorticity Generation by Shock Propagation through Bubbles in a Gas. *J. Fluid Mech.*, 189, 23-51.
- Sears, W. R. (1954). Small Perturbation Theory, Section C, General Theory of High Speed Aerodynamics, Vol. VI, High Speed Aerodynamics and Jet Propulsion. pp 61-121.
- Serdengecti, S. (1992). A General Computational Analysis of Scramjet Performance. Unpublished Notes. California Institute of Technology, Pasadena, California.

Shu, C. W. and Osher, S. J. (1989). Efficient Implementation of Essentially Non-Oscillatory Shock Capturing Schemes, II. *J Comput Phys.*, 83, 32-78.

Ton, V. T. (1993). A New Method of Calculation for Mixing/Chemically Reacting Compressible Flow with Finite Rate Chemistry. Ph.D. Thesis, University of California, Los Angeles. Los Angeles, California

Ton, V. T., Karagozian, A. R., Marble, F. E., Osher, S. J., and Engquist, B. E. (1994). Numerical Simulation of High Speed Chemically Reacting Flow. *Theoretical and Computational Fluid Dynamics*, Vol. 6, pp 161-179.

Waitz, I. A. (1991). An Investigation of Contoured Wall Injectors for Hypervelocity Mixing Augmentation. Ph.D. Thesis, California Institute of Technology, Pasadena California.

Waitz, I. A., Marble, F. E., and Zukoski, E. E. (1992a). A Systematic Experimental and Computational Investigation of a Class of Contoured Wall Fuel Injectors. *AIAA Paper 92-0625*.

Waitz, I. A., Marble, F. E., and Zukoski, E. E. (1992b). Vorticity Generation by Contoured Wall Injectors. *AIAA Paper No. 92-3350*.

Waitz, I. A., Marble, F. E., and Zukoski, E. E. (1993). An Investigation of a Contoured Wall Injector for Hypervelocity Mixing Augmentation. *AIAA J. Prop. and Power*, Vol. 31, No. 6, pp 1014-1021.

Yang, J., Kubota, T., and Zukoski, E.E. (1993). Application of Shock-Induced Mixing to Supersonic Combustion. *AIAA Jour.* Vol 31, No.5, pp 854-862.

Yang, J., Kubota, T., and Zukoski, E.E. (1994). A Model for Characterization of a Vortex Pair Formed by Shock Passage over a Light Gas Inhomogeneity. *J. Fluid Mech.* Vol. 258, 217-244.

Yang, J. and Kubota, T. (1994). The Steady Motion of a Symmetric, Finite Core Size, Counterrotating Vortex Pair. *SIAM J. Appl. Math.* Vol. 54, No. 1, pp 14-25.

## 9. PERSONNEL

### FACULTY

T. Kubota  
F. E. Marble  
E. E. Zukoski

### POST DOCTORAL FELLOWS

G. J. Hendricks  
J. W. Jacobs  
J. D. Sterling

### GRADUATE STUDENTS

J. Kendrick  
M-T. Yueng  
T. W. Zsak  
J. M. Budzinski  
I. A. Waitz  
J. Yang

## 10. PUBLICATIONS, PRESENTATIONS, ETC.

Budzinski, J. M. (1992). Planar Rayleigh Scattering Measurements of Shock Enhanced Mixing. Ph.D. Thesis, California Institute of Technology, Pasadena, California.

Budzinski, J. M. , Zukoski, E. E., and Marble, F. E. (1992). Rayleigh Scattering Measurements of Shock Enhanced Mixing. AIAA Paper No. 92-3546.

Jacobs, J. W. (1992). Shock Induced Mixing of a Light Gas Cylinder J. Fluid Mech., 234, 629-649.

Marble, F. E., Hendricks, G. J., and Zukoski, E. E. (1987). Progress toward Shock Enhancement of Supersonic Combustion Processes. Turbulent Reactive Flows, Rouen, R. Borghi & S.N.B. Murthy (Eds) pp 932-950.

Marble, F. E. (1994). Gasdynamic Enhancement of Non-Premixed Combustion, Proceedings, 25th Symposium, International Combustion Institute, In publication.

Yang, J., Kubota, T., and Zukoski, E.E. (1993). Application of Shock-Induced Mixing to Supersonic Combustion. AIAA Jour. Vol 31, No.5, pp 854-862.

Yang, J., Kubota, T., and Zukoski, E.E. (1994). A Model for Characterization of a Vortex Pair Formed by Shock Passage over a Light Gas Inhomogeneity. J. Fluid Mech. Vol. 258, 217-244.

Yang, J. and Kubota, T. (1994). The Steady Motion of a Symmetric, Finite Core Size, Counterrotating Vortex Pair. SIAM J. Appl. Math. Vol. 54, No. 1, pp 14-25.

Marble, F. E., Zukoski, E. E., Jacobs, J. W., Hendricks, G. J., and Waitz, I. A. (1990). Shock Enhancement and Control of Hypersonic Mixing and Combustion. AIAA Paper No. 90-1981.

Waitz, I. A. (1991). An Investigation of Contoured Wall Injectors for Hypervelocity Mixing Augmentation. Ph.D. Thesis, California Institute of Technology, Pasadena California.

Waitz, I. A., Marble, F. E., and Zukoski, E. E. (1992a). A Systematic Experimental and Computational Investigation of a Class of Contoured Wall Fuel Injectors. AIAA Paper 92-0625.

Waitz, I. A., Marble, F. E., and Zukoski, E. E. (1992b). Vorticity Generation by Contoured Wall Injectors. AIAA Paper No. 92-3350.

Waitz, I. A., Marble, F. E., and Zukoski, E. E. (1993). An Investigation of a Contoured Wall Injector for Hypervelocity Mixing Augmentation. AIAA J. Prop. and Power, Vol. 31, No. 6, pp 1014-1021.

All of the above publications involved public presentations. The following, however, deserve special mention.

March 4, 1988, University of California, Irvine. Shock Enhanced Mixing Applied to Supersonic Combustion Ramjets. Frank E, Marble.

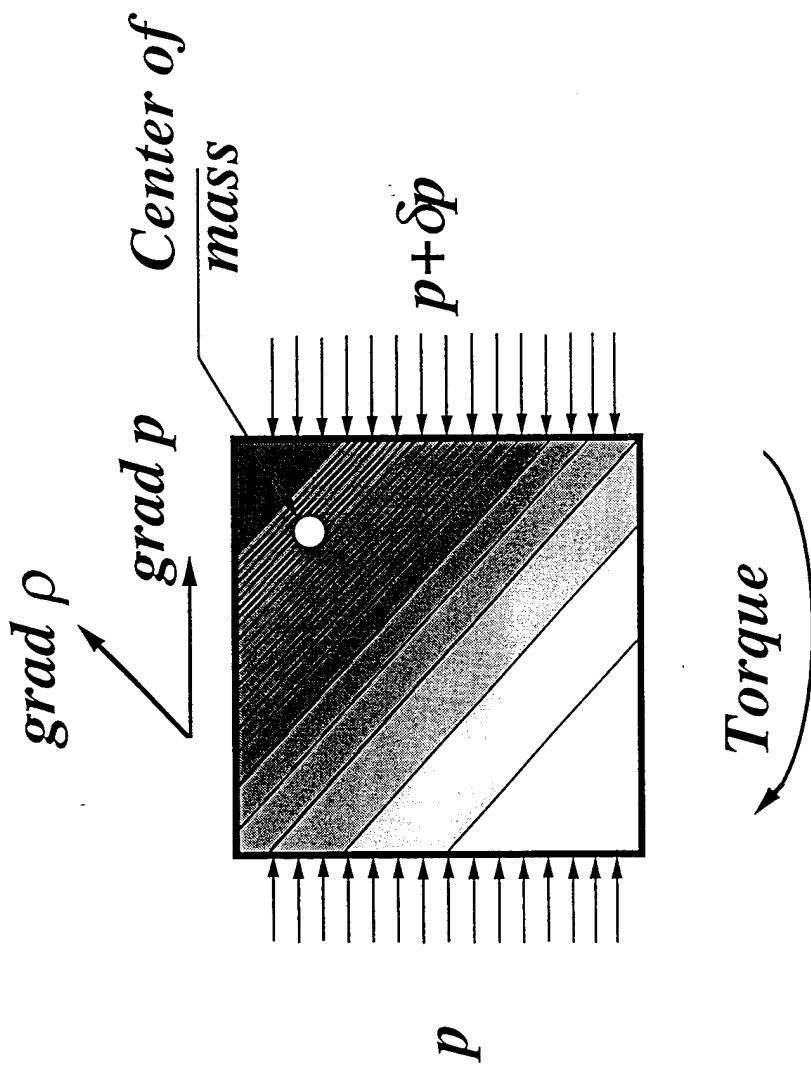
April 19, 1990, Cornell University, Ithaca New York. The W. R. Sears Distinguished Lecture. "Rapid Mixing and Combustion - A Challenge of Hypersonic Flight" Frank E. Marble

October 5, 1990, Ohio Aerospace Institute, Cleveland. The Parker Hannifin Distinguished Lecture. "Rapid Mixing and Combustion - A Challenge of Hypersonic Flight" Frank E. Marble

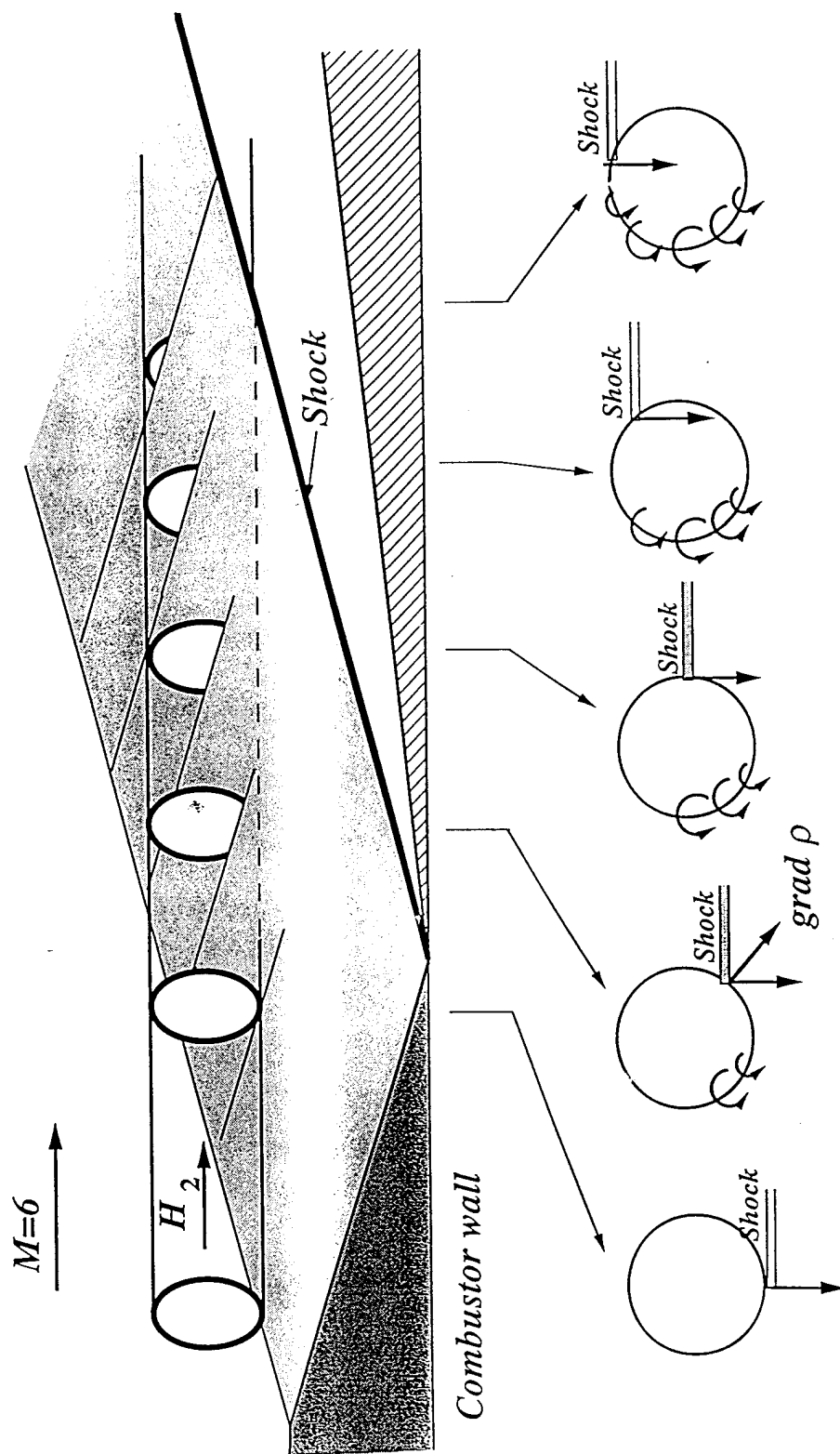
August 1, 1994, 25th Symposium, International Combustion Institute, Irvine California. The Hottel Plenary Lecture. "Gasdynamic Enhancement of Non-Premixed Combustion" Frank E. Marble

Invention: Contoured Wall Injector for Hypervelocity Mixing.

Date of Disclosure: September 13, 1989.



1. Vorticity Generation in a Gas of Non-Uniform Density



2. Progression of Shock through the Hydrogen Jet

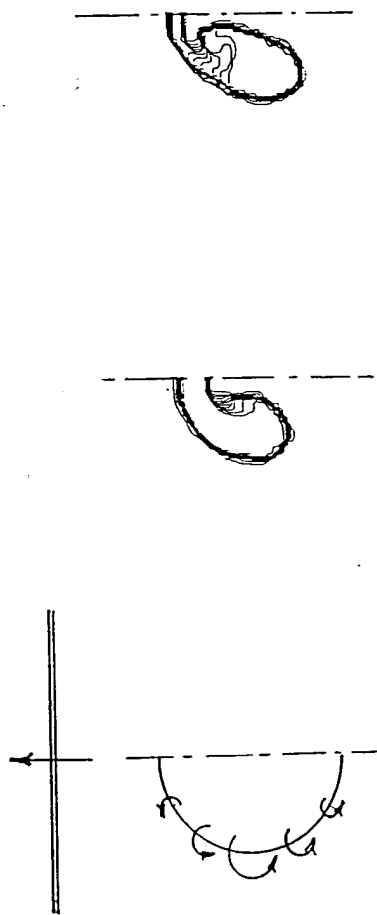


Figure 3. Distortion of Hydrogen Cylinder after Shock Passage  
and Subsequent Formation of Vortex Pair

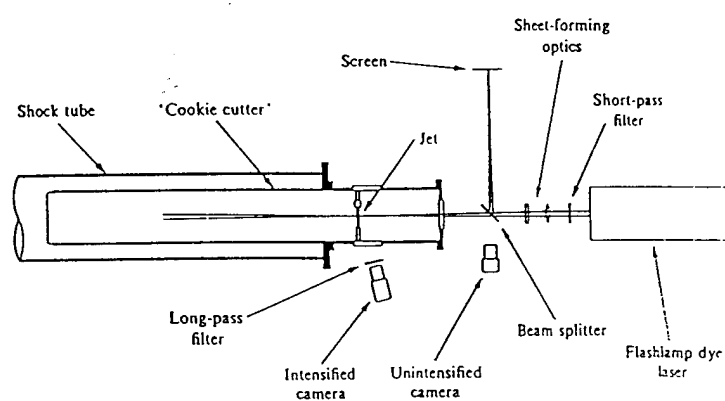
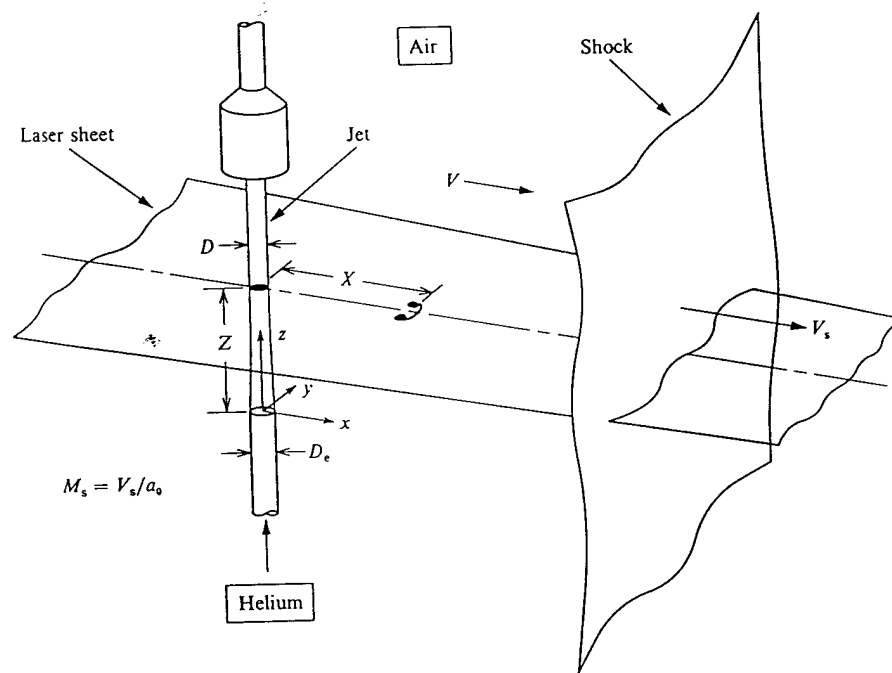
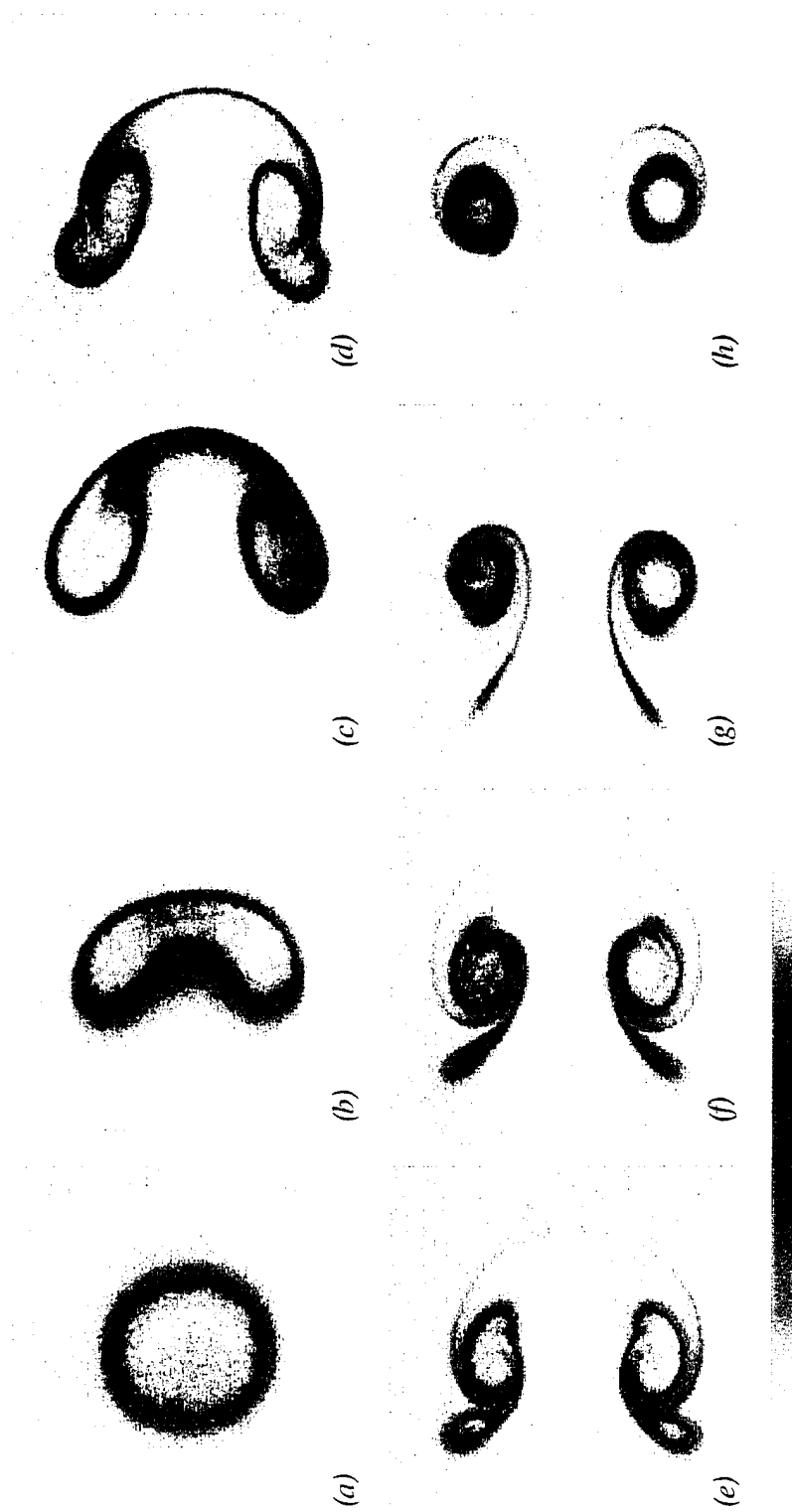


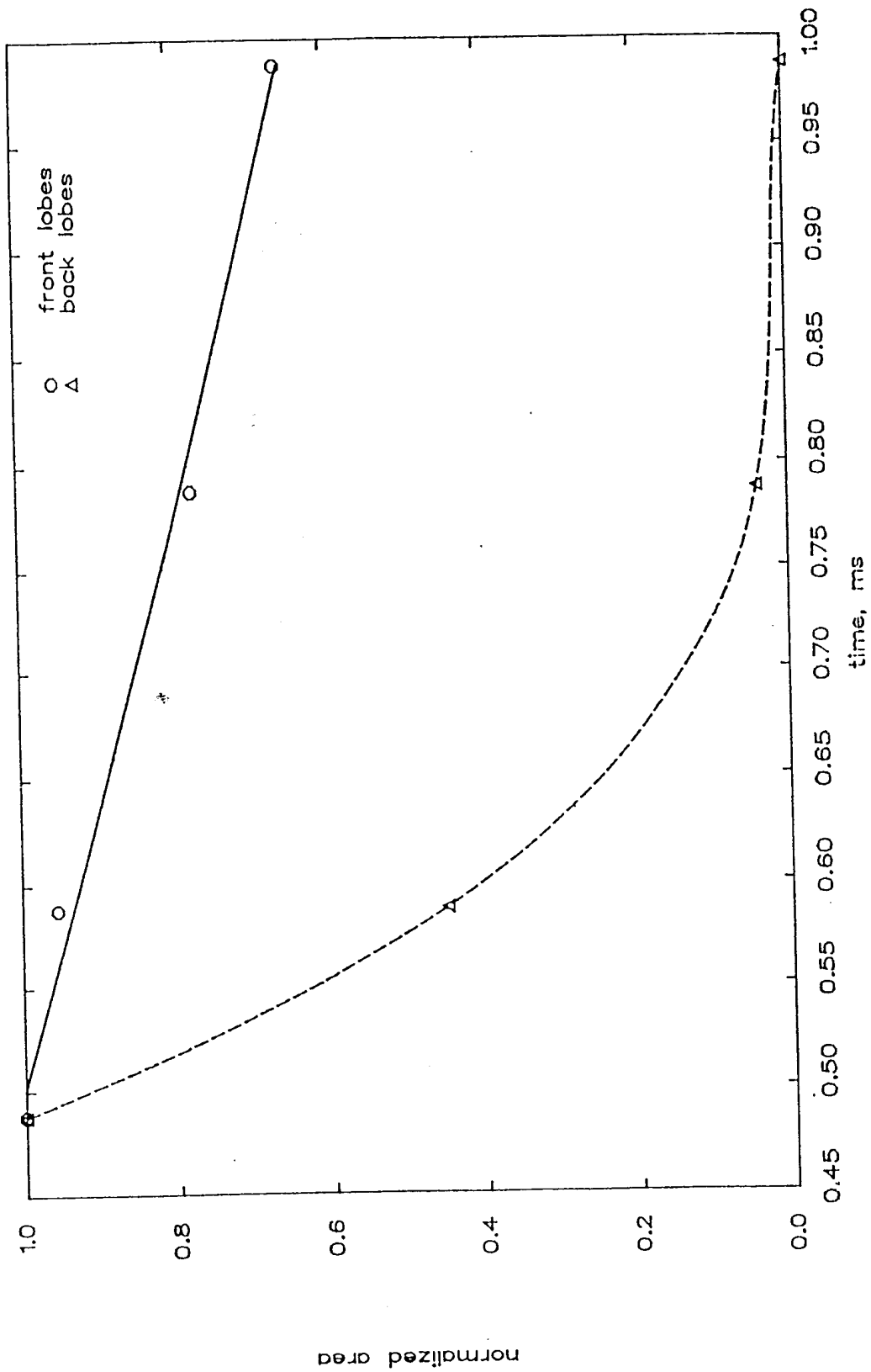
Figure 4. Working Section and Laser Induced Fluorescence System



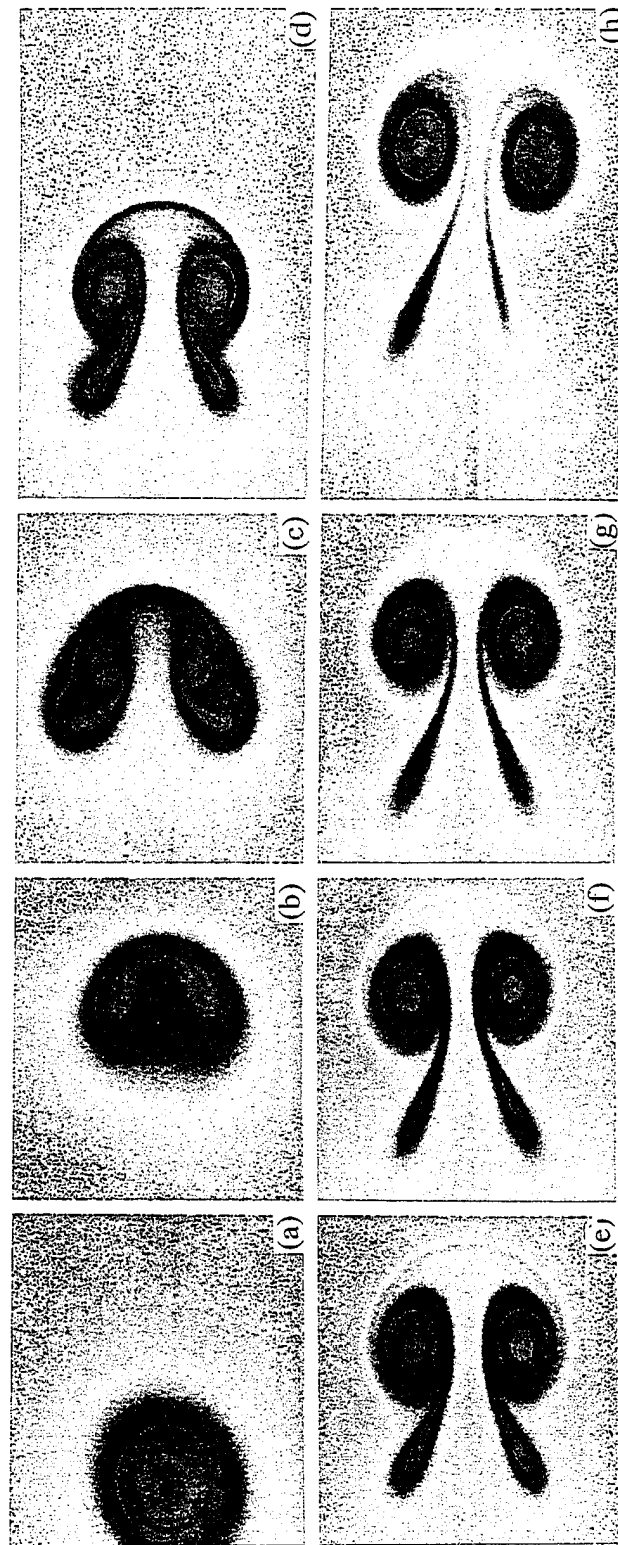
5. The Jet/PLIF Configuration



6. Time Sequence of PLIF Images of the Distortion and Mixing of Helium Jet after Encounter with  $M_s = 1.093$  Shock. (a) The initial jet, (b) 0.123 ms, (c) 0.273 ms, (d) 0.373 ms, (e) 0.473 ms, (f) 0.573 ms, (g) 0.773 ms, (h) 0.973 ms.

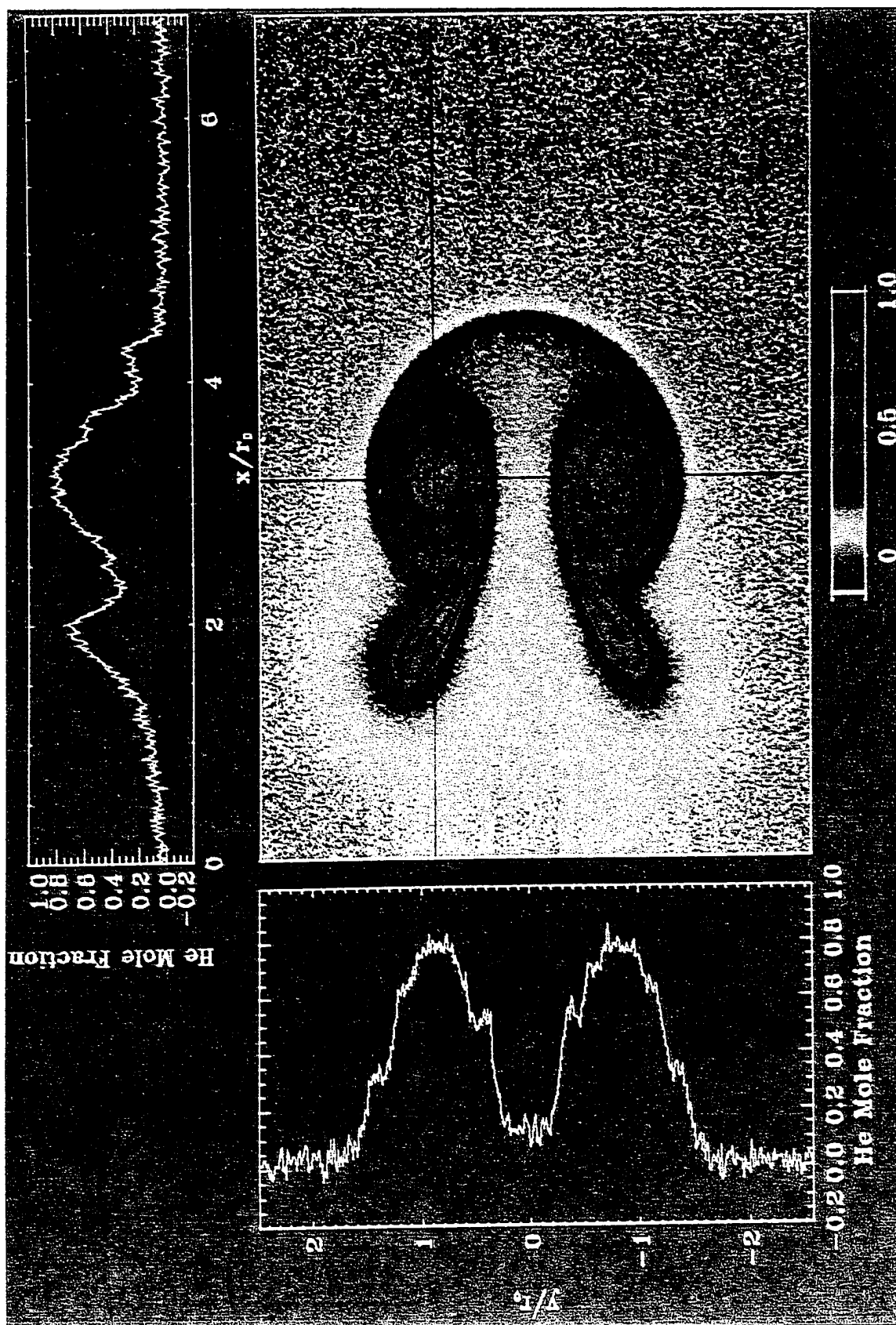


7. Time History of Forward and Rearward Lobes

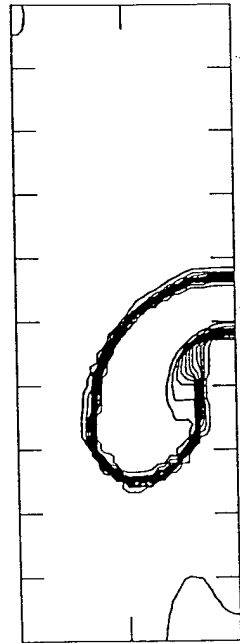


8. Rayleigh Scattering Images of Weak Shock Interaction with Helium Jet,  $M_g = 1.066$

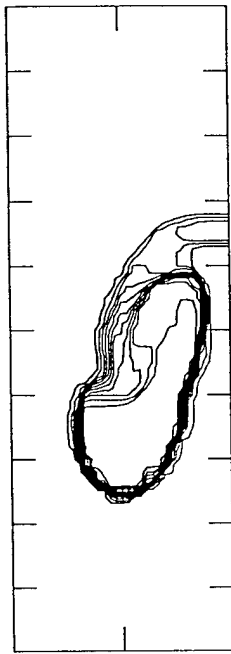
a) $t = 0.0$ ms	c) $t = 0.70$ ms	d) $t = 1.15$ ms
e) $t = 1.72$ ms	f) $t = 1.89$ ms	g) $t = 2.13$ ms
		h) $t = 2.64$ ms



9. Rayleigh Scattering Image and Distributions of Helium Density



a)



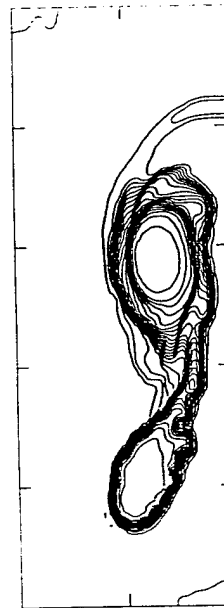
b)



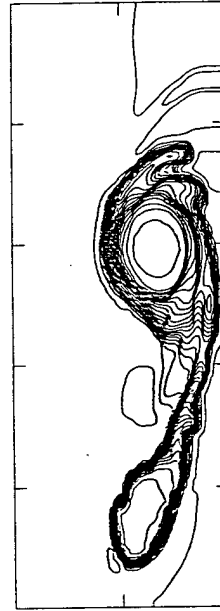
c)



d)



e)



f)

10. Time Sequence of Computed Density Contours,  $M_s = 1.22$

a)  $t = 0.43$  ms

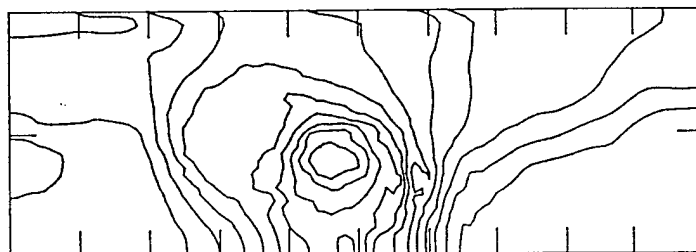
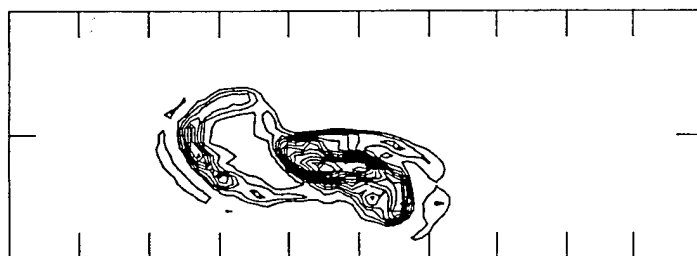
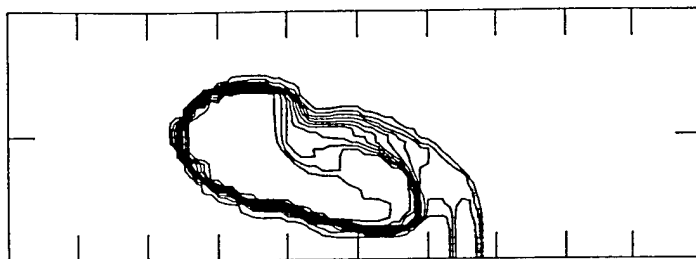
b)  $t = 0.83$  ms

c)  $t = 1.09$  ms

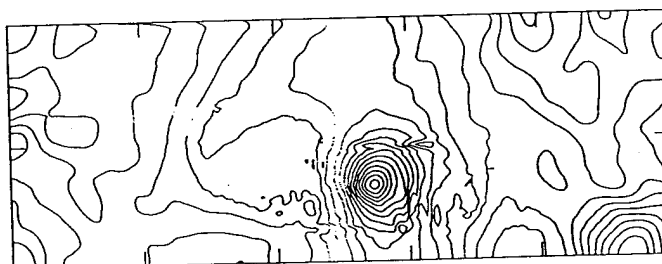
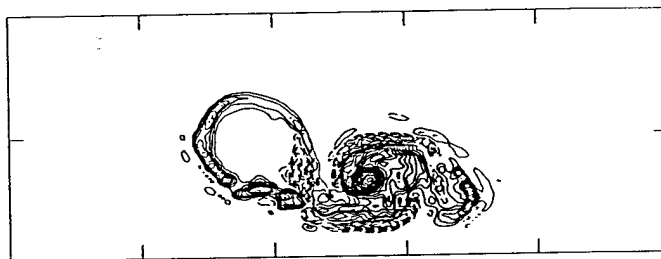
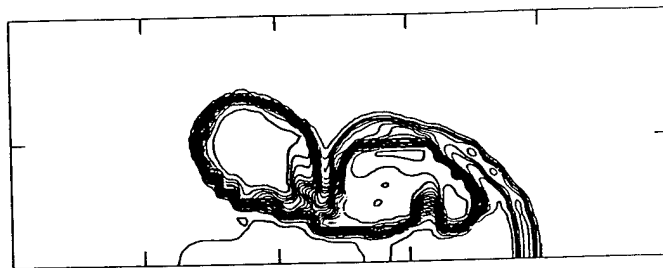
d)  $t = 1.47$  ms

e)  $t = 1.82$  ms

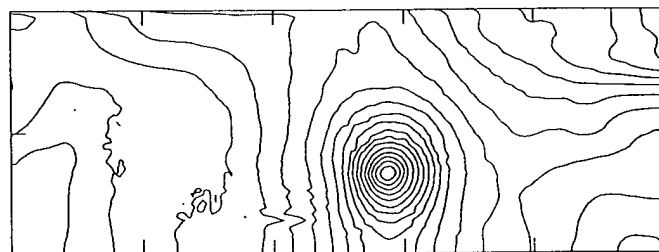
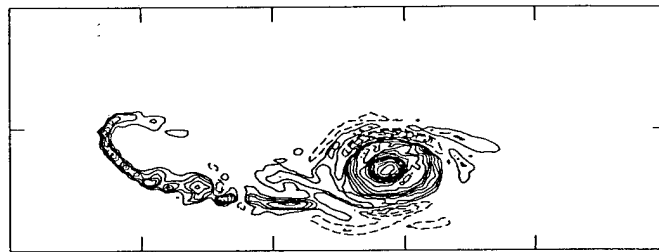
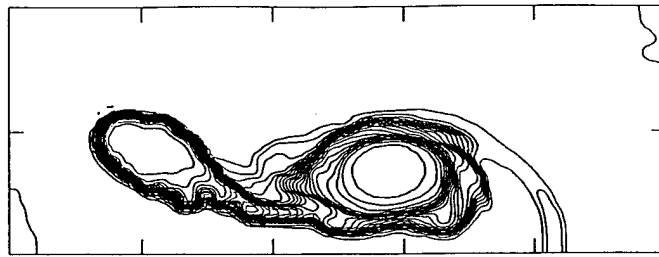
f)  $t = 2.20$  ms



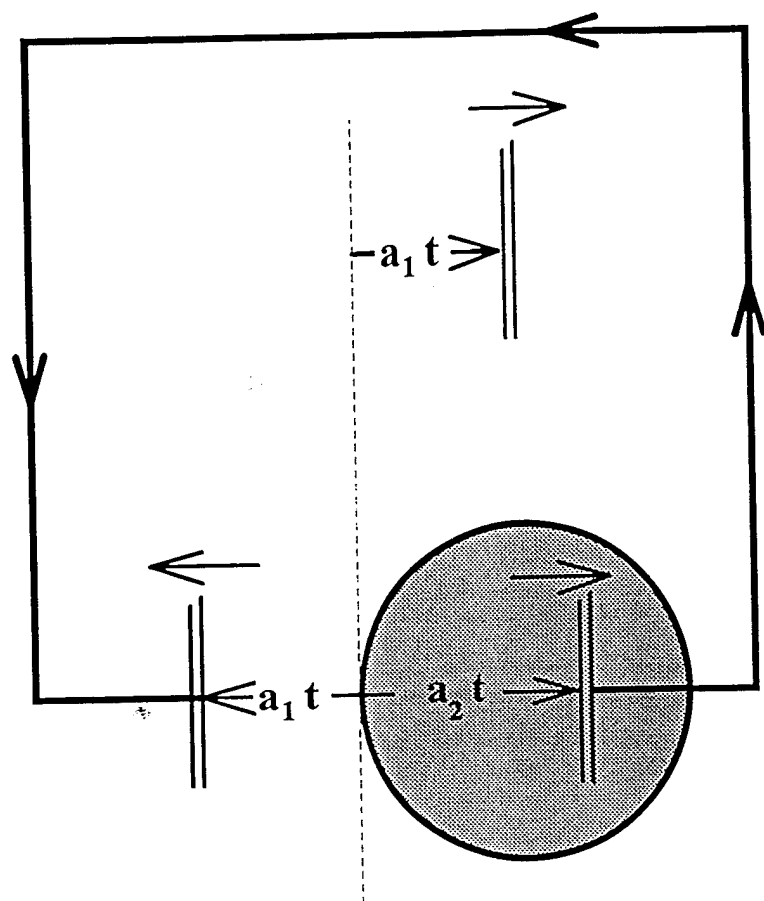
11. Computed Density, Vorticity, and Pressure Contours,  $M_s = 1.22$   
 $t = 0.83$  ms



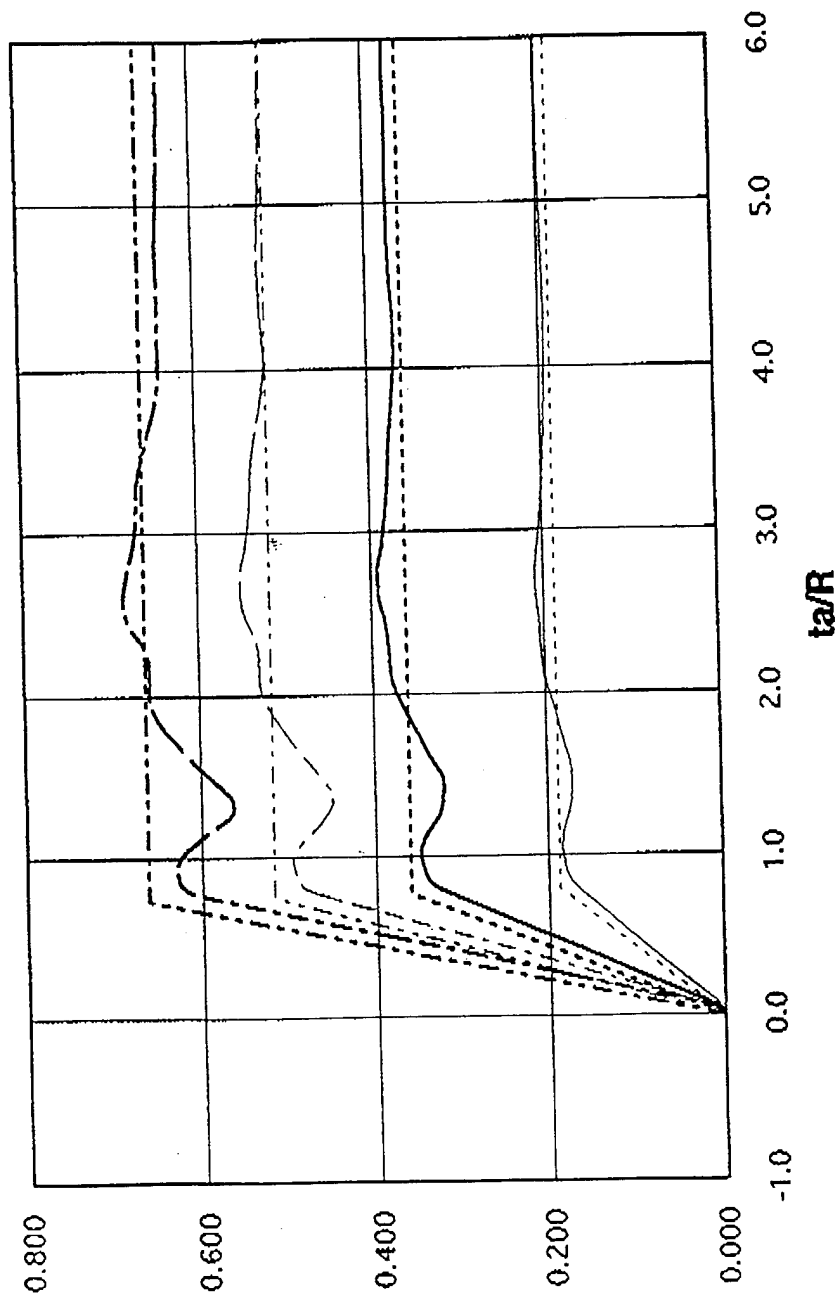
12. Computed Density, Vorticity, and Pressure Contours,  
 $M_s = 1.22$   
 $t = 1.09 \text{ ms}$



13. Computed Density, Vorticity, and Pressure Contours,  
 $M_s = 1.22$   
 $t = 1.82 \text{ ms}$



14. Contour for Circulation Calculation



15. Circulation Growth from Euler Code and Approximate Analysis



a

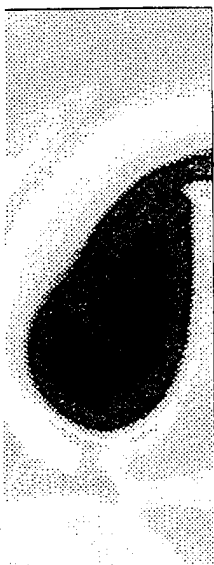


b



c

Non Reacting



A



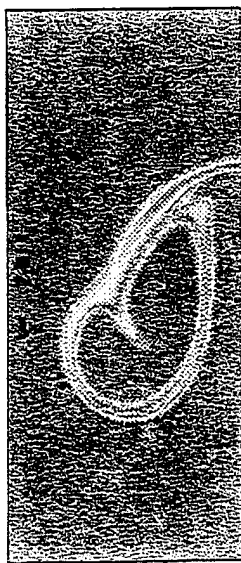
B



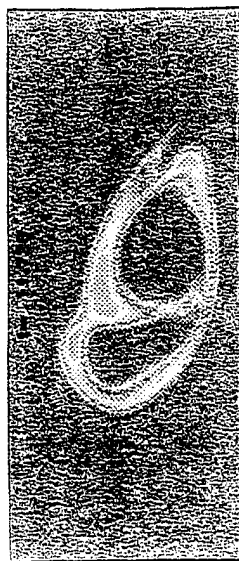
C

Reacting

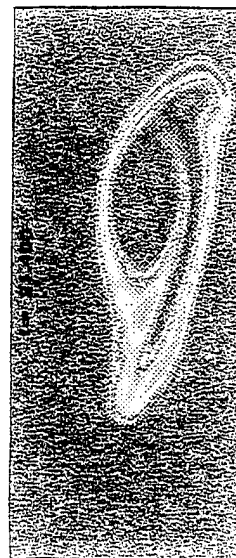
16. Computed Density Contours for Reacting and Non Reacting Flow,  
Initial Temperature 1000°K,  $M_s = 1.22$



a



b

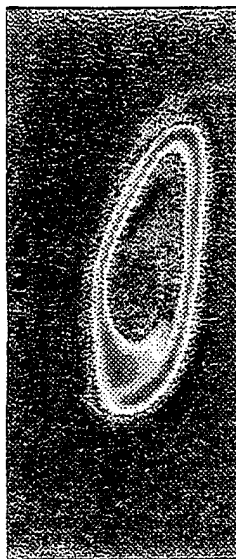


c

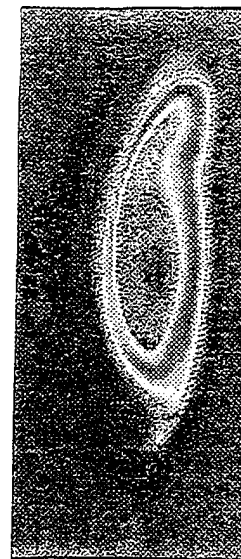
10000 K



A



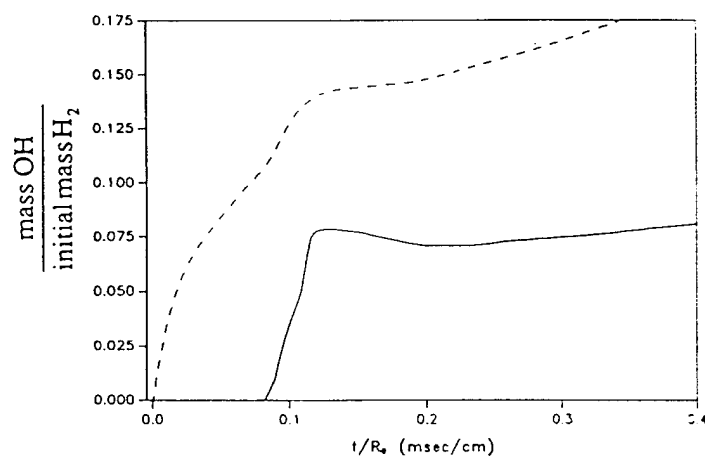
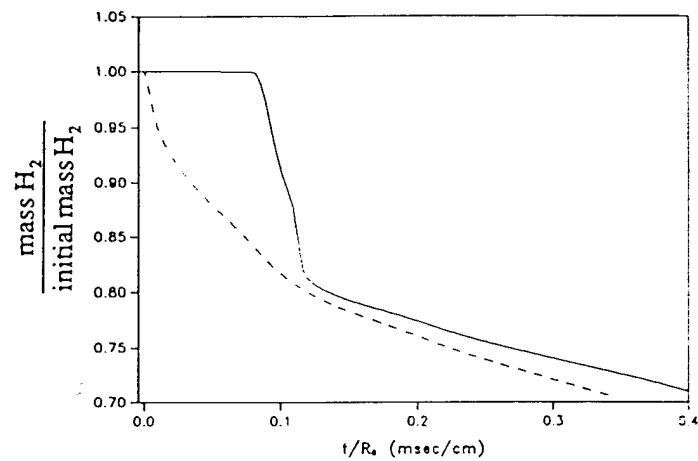
B



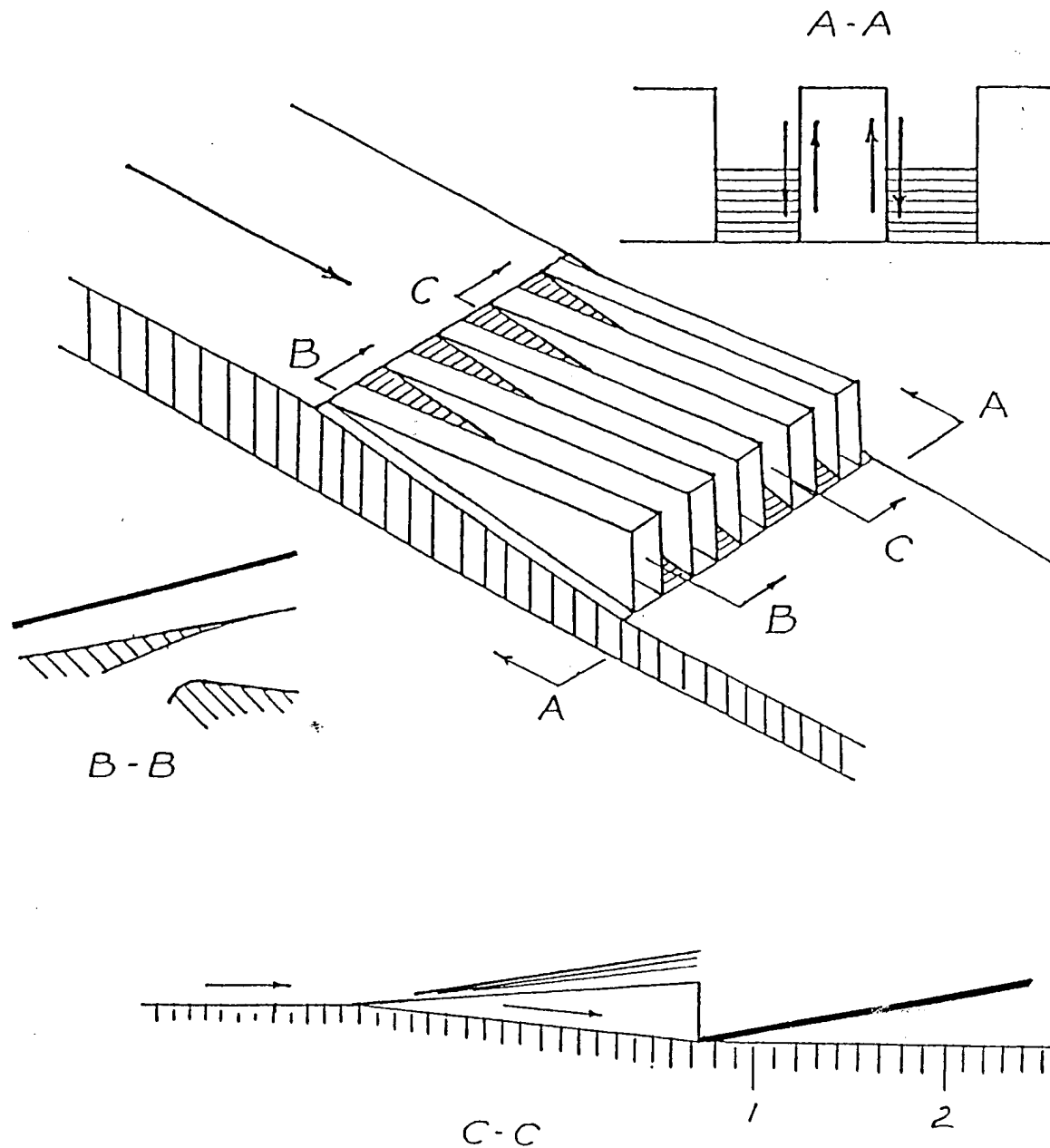
C

15000 K

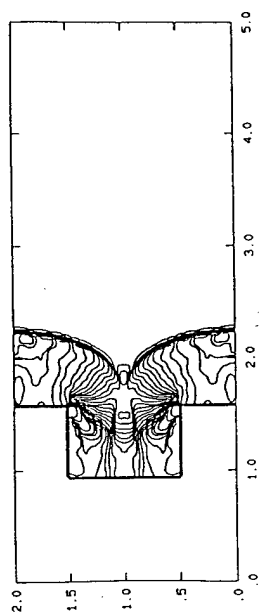
17. Computed Temperature Contours, Initial Temperature 1000°K, 1500°,  $M_s = 1.22$



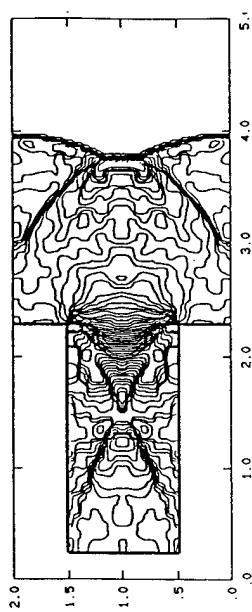
18. Consumption/Growth Histories of  $H_2$  and OH,  
Initial Temperatures  $1000^\circ \text{K}$ ,  $1500^\circ \text{K}$



19. Sketch of Wall Mounted Hydrogen Injector Utilizing Shock Enhanced Mixing



a)

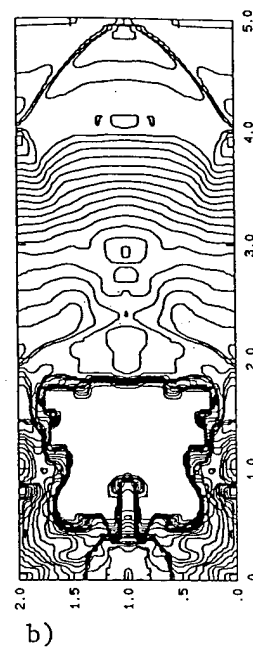
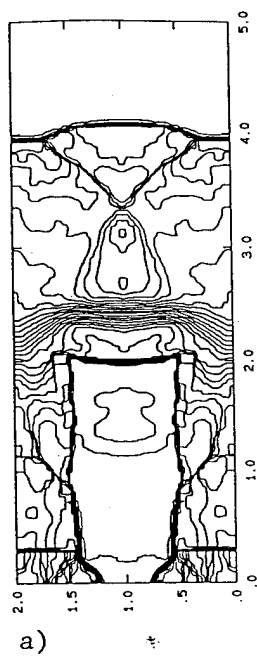


b)

## 20. Development of Flow Field within the Injector Trough

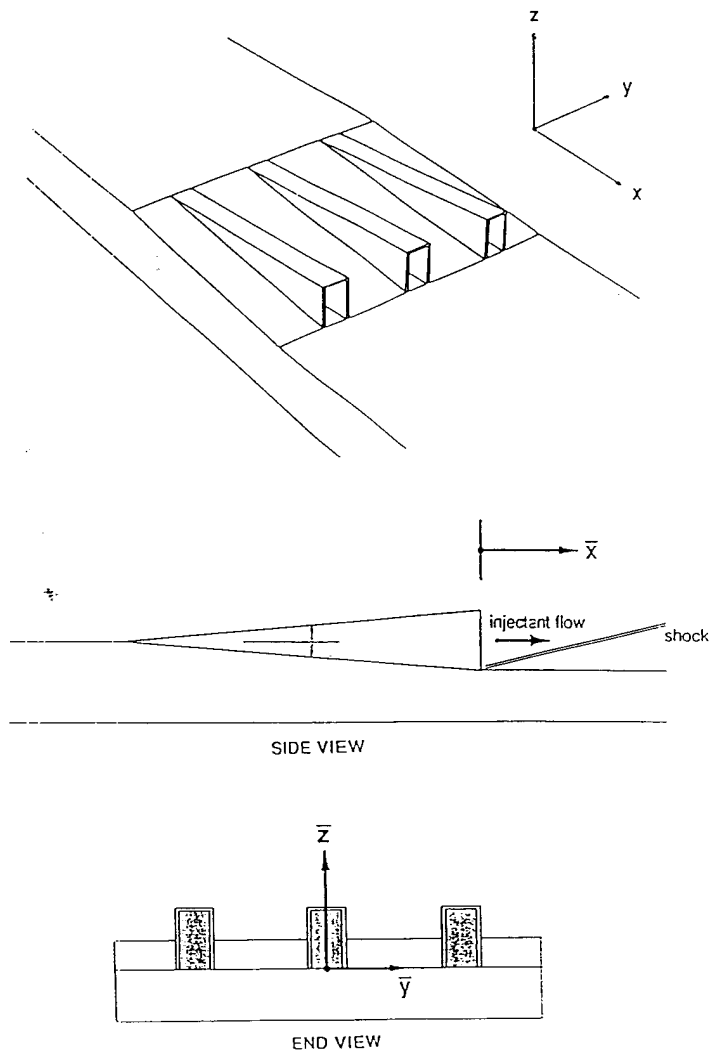
a)  $x=4$

b)  $x=12$

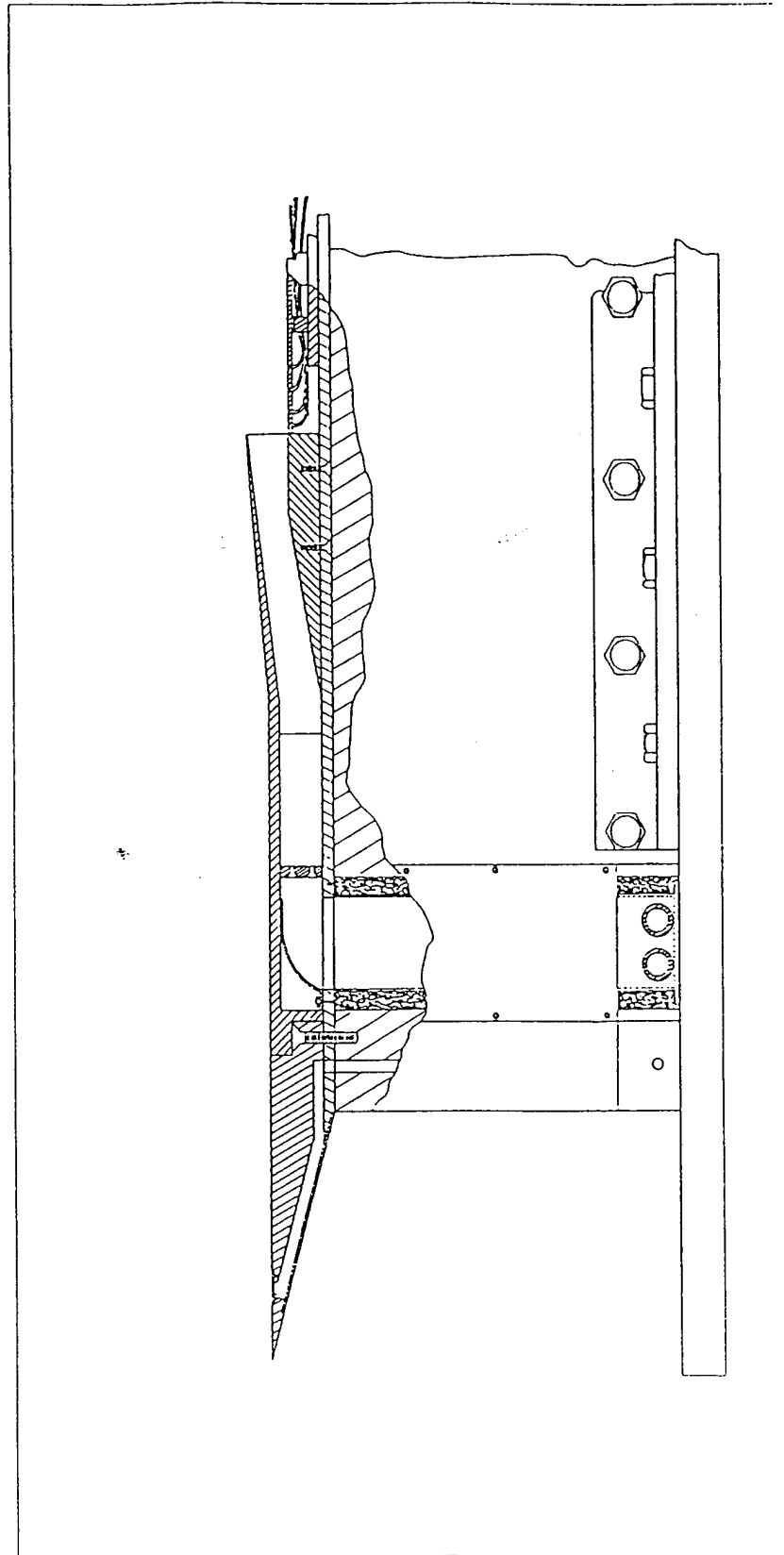


21. Development of the Streamwise Vortex Pair Downstream of the Injector

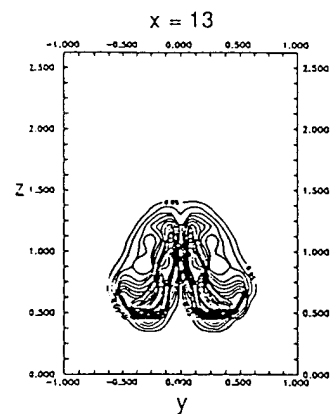
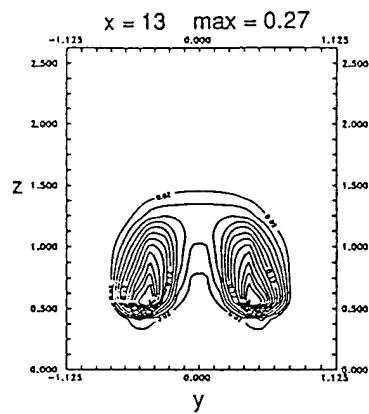
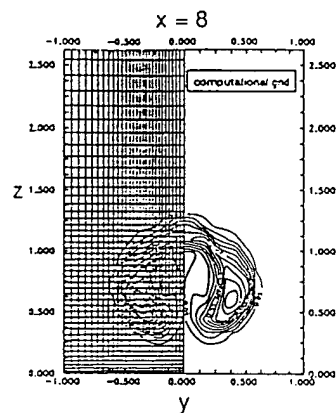
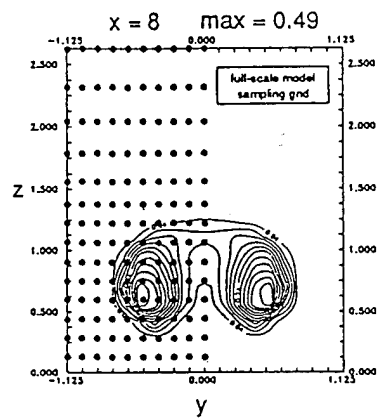
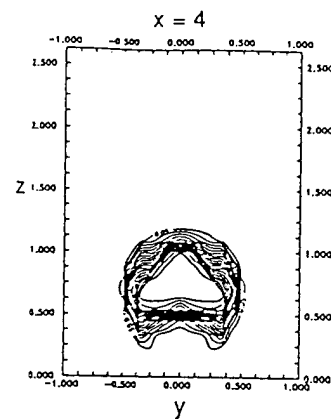
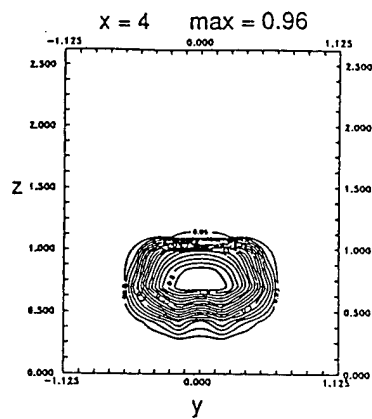
- a)  $x=14$
- b)  $x=20$



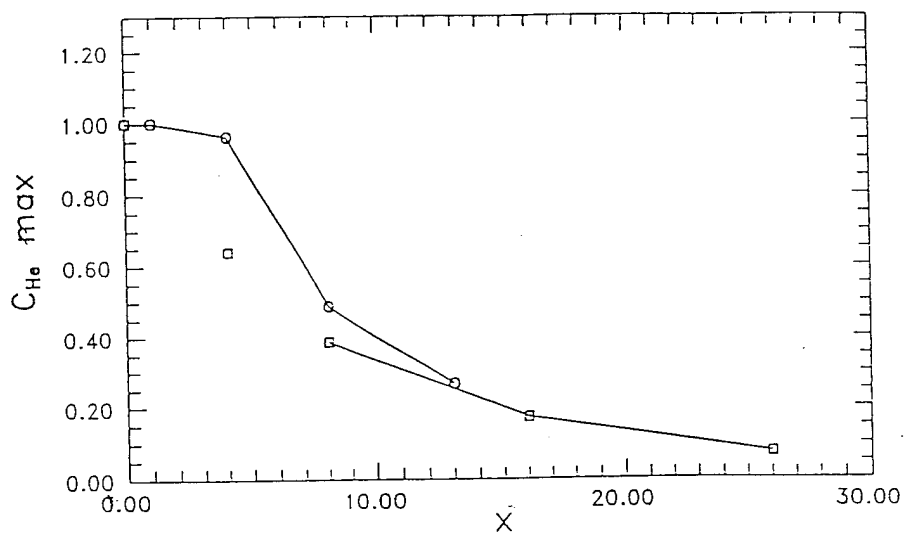
22. Drawing of Model Injector



23. Cross Section of Model Injector in Tunnel Mounting



24. Experimental and Computational Contours of Helium Mass Fraction



25. Measured Decay of Maximum Helium Concentration along Flow Direction